Russian Chemical Reviews **71** (8) 651 – 671 (2002) © 2002 Russian Academy of Sciences and Turpion Ltd

DOI 10.1070/RC2002v071n08ABEH000716

Barium borate β-BaB_2O_4 as a material for nonlinear optics

P P Fedorov, A E Kokh, N G Kononova

Contents

I.	Introduction	651
II.	Barium borates. The $BaO - B_2O_3$ system	652
III.	Glass formation in the $BaO - B_2O_3$ system	655
IV.	Methods of preparation of BaB_2O_4	655
V.	Polymorphism and the crystal structure	657
VI.	Peculiarities of crystallisation of BaB_2O_4 melts	659
VII.	Growth of β-BaB_2O_4 single crystals	660
VIII.	Defects and impurities in crystals	665
IX.	Constitutional supercooling	666
X.	Properties and fields of application of β-BaB_2O_4 crystals	667
XI.	Conclusion	668

Abstract. Data on the structure, polymorphism, phase equilibria, growth techniques, properties and applications of single crystals of the low-temperature modification of barium borate are analysed. The bibliography includes 201 references.

I. Introduction

Barium borates possess many interesting and valuable properties. Interest in these compounds is due to not only pure research aspects, but also the possibility of modern technological applications. Currently, barium borates are used in production of ceramic glazes, luminophors, oxide cathodes as well as additives to pigments for aqueous emulsion paints.[1–8] The $BaO - B_2O_3$ system (a constituent of the $BaO - B_2O_3 - SiO_2$ system) serves as the basis when synthesising special optical glasses.[9–14]

The history of studies of barium borate, BaB_2O_4, can be divided into two periods. The pioneering communication concerning the synthesis of BaB_2O_4 single crystals dates back to the 19th century.[1,2] The structure of anions in crystalline borates was established by X-ray structural analysis in the 1950s.[3,4,15] The crystal structures of a number of barium borates including the high-temperature modification of BaB_2O_4 were established in the 1960s;[16–18] however, these results were of low reliability.

Two crystalline modifications† of BaB_2O_4, *viz*., the high-temperature (α) and the low-temperature (β) forms were described and characterised by X-ray diffraction analysis by Levin and McMurdie.[12]

In the anions, oxygen atoms surrounding borons can form two types of coordination environment, *viz*., a tetrahedral and a trigonal coordination environment corresponding to the sp^3- and sp^2-hybridisation of the electron orbitals of the B atom, respectively.[19] As a rule, both of them are realised in borate ions. Both the BO_3 triangles and BO_4 tetrahedra can form fused structures by sharing their vertices (bridging oxygen atoms), thus forming polyanions. The presence of polymeric anions in borate melts is responsible for hysteresis of properties (in particular, viscosity) and the glass-forming ability.[8]

The second period of studies of BaB_2O_4 dates back to the 1980s and is associated with the discovery of nonlinear optical properties in the single crystals of the low-temperature modification of barium borate, β-BaB_2O_4 (BBO)‡ (see Refs 20–25). Its crystals are non-centrosymmetric, which is responsible for a number of specific properties of the compound.[26,27] This form of barium borate combines excellent nonlinear optical characteristics [large effective second harmonic generation (SHG) coefficient, which is nearly 6 times higher than that of potassium dihydrophosphate crystals; large birefringence; wide transparency region (190–3500 nm), high laser damage threshold], good mechanical properties and very low hygroscopicity. Comparison of the properties of BBO with those of other optically active nonlinear crystals shows that barium borate is the best candidate for fabrication of solid-state UV lasers operating at a wavelength of 200 nm. BBO single crystals are used in optoelectronics for laser radiation-to-radiation frequency conversion (in particular, visible-to-UV frequency upconversion) by the SHG and higher harmonic generation (up to the fifth harmonic) mechanisms.

P P Fedorov A V Shubnikov Institute of Crystallography, Russian Academy of Sciences, Leninsky prosp. 59, 119991 Moscow, Russian Federation. Fax (7-095) 135 10 11. Tel. (7-095) 330 78 74.
E-mail: ppf@newmail.ru
A E Kokh, N G Kononova Institute of Mineralogy and Petrography, Siberian Branch of the Russian Academy of Sciences, prosp. Acad. Koptuga 3, 630090 Novosibirsk, Russian Federation.
Fax (7-383) 233 27 92. Tel. (7-383) 233 39 47. E-mail: kokh@mail.ru

Received 14 March 2002
Uspekhi Khimii **71** (8) 741 – 763 (2002); translated by A M Raevsky

† In the literature, the high-temperature and the low-temperature modifications of barium borate are, as a rule, designated as α-BaB_2O_4 and β-BaB_2O_4, respectively (in this review, we also use these notations). However, quite the reverse notations are sometimes used.

‡ The terminology is somewhat ambiguous. The compound having a composition $BaO \cdot B_2O_3$ is usually treated as a salt, $Ba(BO_2)_2$, of metaboric acid (HBO_2) and called barium metaborate;[2] sometimes, the same compound is called barium diborate (see, *e.g*., Ref. 4). However, barium diborate has another composition, namely, $BaO \cdot 2\,B_2O_3$.[2] To match the crystal structure of BBO, it is more correct to represent its composition as $Ba_3(B_3O_6)_2$.

Recently, frequency conversion by the stimulated Raman scattering (SRS) mechanism using BBO-crystal oscillators has been studied.[28–30]

In the last decade, new crystals possessing nonlinear optical properties (including borates) were synthesised.[31–39] These are, *e.g.*, LiB_3O_5 (LBO)§ (see Ref. 31), $KBe_2BO_3F_2$ (KBBF),[32] $Sr_2Be_2B_2O_7$ (SBBO),[33] $LiCsB_6O_{10}$ (CLBO),[34] $Ba_2Be_2B_2O_7$ (TBO) and $K_2Al_2B_2O_7$ (KABO)[35] and $BiBO_3$ (BIBO);[36] however, BBO remains of considerable value.

Nonlinear optical properties of various borate single crystals are due to electron delocalisation[37,38,40–43] in complex boron–oxygen anions. The simplest examples of such anions are provided by the $[BO_3]^{3-}$ triangles and by two types of ring trimers, *viz.*, the $[B_3O_6]^{3-}$ units constructed of three BO_3 triangles with two of the three vertices shared and the $[B_3O_7]^{5-}$ units (two BO_3 triangles linked by the BO_4 tetrahedron). They are shown in Fig. 1. Peculiarities of the electronic structure of borate crystals determine high polarisability of these compounds, which is comparable to that of aromatics. These crystals also have good mechanical properties and high laser damage threshold, which is typical of inorganic crystals.[44]

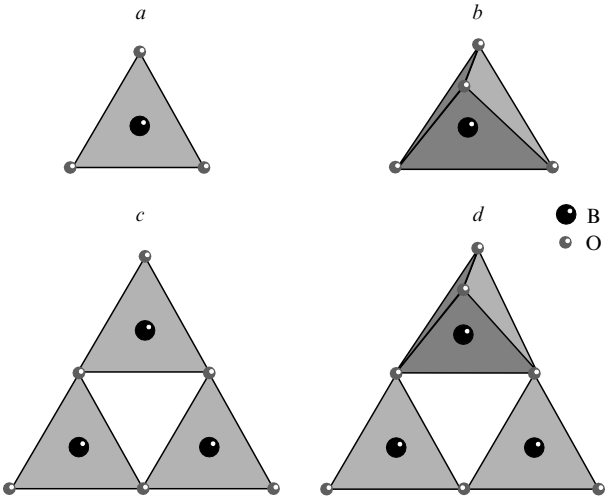


Figure 1. Structural units present in borate crystals.
BO_3 (*a*); BO_4 (*b*); B_3O_6 (*c*) and B_3O_7 (*d*).

Solid-state optoelectronics (photonics) requires high-quality crystals that contain no inclusions, twins and inhomogeneities, are free from thermal strain and variations of the refractive index, have a definite crystallographic orientation and are, as a rule, rather large (of the order of a centimetre). BBO single crystals can be grown by melt-solution (high-temperature flux) technique using the modified Kyropoulos and Czochralski methods[45,46] or by direct crystallisation from supercooled melts. Crystal growth is complicated by high viscosity and glass-forming ability of melts. The polymeric structure of borate melts can be to some extent controlled by shifting the acid–base equilibria.[47,48] Low yield of materials suitable for practical applications, undesired variations of the properties of BBO crystals and high cost of optical elements are due to the fact that growing such crystals is a technologically sophisticated procedure.

Recently, interest to centrosymmetric single crystals of the high-temperature α-modification of BaB_2O_4 has quickened.[49] These crystals are characterised by large birefringence, broad optical transparency region (190–3500 nm) and can compete with calcite crystals that are widely used in linear optics.

An extensive literature on BBO crystals has evolved. Despite this fact, a number of topical problems concerning both the basic (nonstoichiometry, polymorphism, phase equilibria, thermodynamics) and applied (elucidation of the reasons responsible for characteristic optical and structural inhomogeneities of BBO crystals, optimisation of crystal growth conditions) aspects of the investigation and growth of these crystals are still to be solved.

§ The notations widely used in the literature are given in parentheses.

II. Barium borates. The $BaO-B_2O_3$ system

Studies of the phase equilibria in the $BaO-B_2O_3-H_2O$ system at 30 °C (Fig. 2) revealed the existence of barium metaborate tetrahydrate, $BaO\cdot B_2O_3\cdot 4H_2O$, and barium triborate heptahydrate, $BaO\cdot 3B_2O_3\cdot 7H_2O$.[2,50] Some other hydrated barium borates were reported in the early studies.[2] More recently,[4] $BaO\cdot B_2O_3\cdot 5H_2O$ was synthesised, which is formed in dilute solutions and is thought to be metastable,[5] as well as $BaB_2O_4\cdot 1.67H_2O$.[51] Determination of the crystal structures of $BaO\cdot B_2O_3\cdot 4H_2O$ (see Ref. 52) and $BaO\cdot B_2O_3\cdot 5H_2O$ (see Refs 53 and 54) revealed the presence of isolated tetrahedral $B(OH)_4$ groups in these crystals; therefore, the formulae of the compounds can be written as $Ba[B(OH)_4]_2$ and $Ba[B(OH)_4]_2\cdot H_2O$, respectively.

The crystalline compounds $Ba_2[B_5O_8(OH)_2]OH$, $Ba[B_5O_8(OH)]\cdot H_2O$ and $Ba_5[B_{20}O_{33}(OH)_4]\cdot H_2O$ were hydrothermally synthesised in the $BaO-B_2O_3-M_2O-H_2O$ (M = K, Rb, Cs) systems at 280 °C under a pressure of 70 atm.[55–58]

The melting diagram of the $BaO-B_2O_3$ system was studied by thermal analysis.[59,60] Using the 'composition–property' curve, six congruently melting compounds were found. These are $3BaO\cdot B_2O_3$, $2BaO\cdot B_2O_3$, $BaO\cdot B_2O_3$, $BaO\cdot 2B_2O_3$,

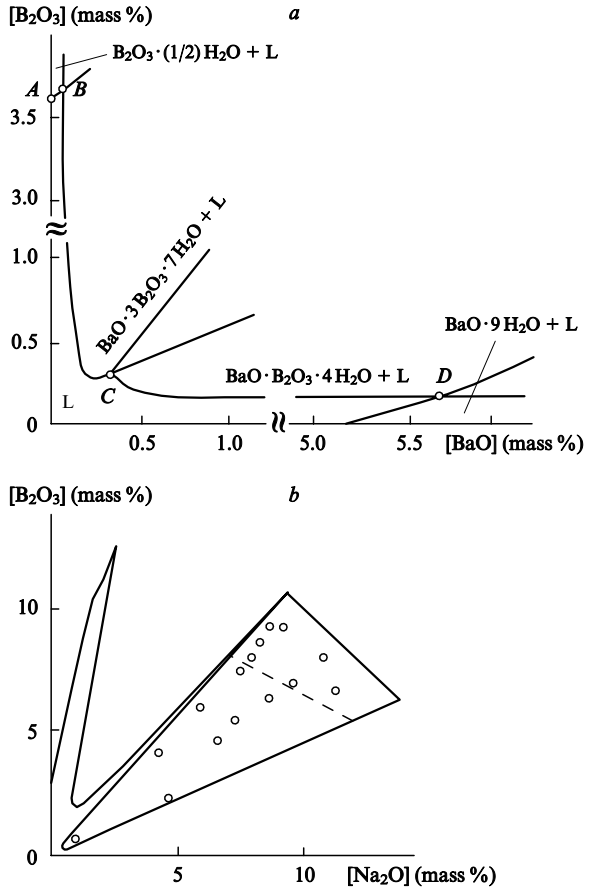


Figure 2. Phase equilibria in the $BaO-B_2O_3-H_2O$ system at 30 °C (*a*)[2,50] and crystallisation field of $BaB_2O_4\cdot nH_2O$ (open circles) in sodium borate solutions at 25 °C (*b*).[5]
Points *B*, *C* and *D* denote eutonics (*a*); the dashed line designates the boundary between the tetrahydrate and pentahydrate regions (*b*).

$BaO \cdot 3\,B_2O_3$ and $BaO \cdot 4\,B_2O_3$ (for the generalised phase diagram of the $BaO - B_2O_3$ system, see Ref. 2). It is believed that supercooling of melts occurred in these studies.

Phase equilibria in the $BaO - B_2O_3$ system have been studied in detail [12] by annealing and quenching techniques and by the X-ray phase and thermal analyses. Only four congruently melting compounds were found, namely, $3\,BaO \cdot B_2O_3$, $BaO \cdot B_2O_3$, $BaO \cdot 2\,B_2O_3$ and $BaO \cdot 4\,B_2O_3$. A melt immiscibility region was observed near the boron oxide composition.

Barium metaborate, $BaO \cdot B_2O_3$, melts congruently at 1095 °C and forms eutectics at 905 and 889 °C.[12] In addition to the high-temperature α-modification of $BaO \cdot B_2O_3$, the low-temperature β-modification was found and characterised by X-ray powder diffraction. No transition temperature was reported;[12] it was only assumed to lie between 100 and 400 °C. More recently, in studies of the $BaO - B_2O_3 - SiO_2$ ternary system[13] the temperatures of a number of phase transformations in the $BaO - B_2O_3$ system were corrected (increased by ~10 °C) while the melting temperature of $BaO \cdot B_2O_3$ was found to be 1105 °C.

The generalised phase diagram of the $BaO - B_2O_3$ system (Fig. 3), which was proposed by Levin and reported in a handbook,[10] has been commonly accepted by crystal growth researchers (see, *e.g.*, Refs 11, 27, 46). Following Feigelson *et al.*,[46] in Fig. 3 we added a horizontal line (dash-and-dot line) corresponding to the polymorphic transformation of $BaO \cdot B_2O_3$ at 925 °C (see below). It should be noted that the boundaries of the immiscibility region (dashed line) do not match those reported earlier.[12] The coordinates of the upper critical point of the immiscibility dome (1931 °C, 6.6 mol.% BaO) were determined in a thorough study by Hageman and Oonk.[61]

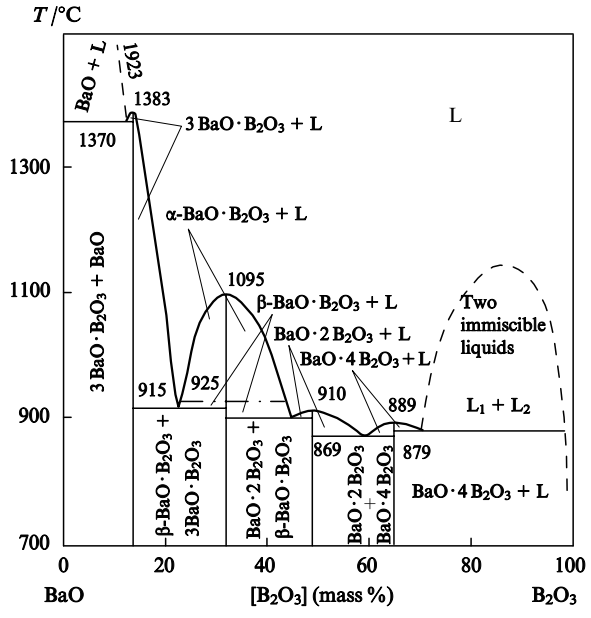


Figure 3. Phase diagram of the $BaO - B_2O_3$ system.[10]

The middle part of the phase diagram of the $BaO - B_2O_3$ system was revised by Hübner [62] who showed that not only the above-mentioned compounds, but also $2\,BaO \cdot 5\,B_2O_3$, $2\,BaO \cdot B_2O_3$ and $4\,BaO \cdot B_2O_3$ are formed in the system. All of the newly found compounds were characterised by X-ray powder diffraction. The congruent melting temperature of $2\,BaO \cdot B_2O_3$ (920 ± 5 °C) is close to the temperature of the eutectic between $BaO \cdot B_2O_3$ and $3\,BaO \cdot B_2O_3$.[12, 13] The temperature of the polymorphic transformation of $BaO \cdot B_2O_3$ is 925 ± 5 °C. Hübner proposed the existence of homogeneity regions for both modifications of $BaO \cdot B_2O_3$ and suggested that this region for the high-temperature form is especially broad (Fig. 4). According to this

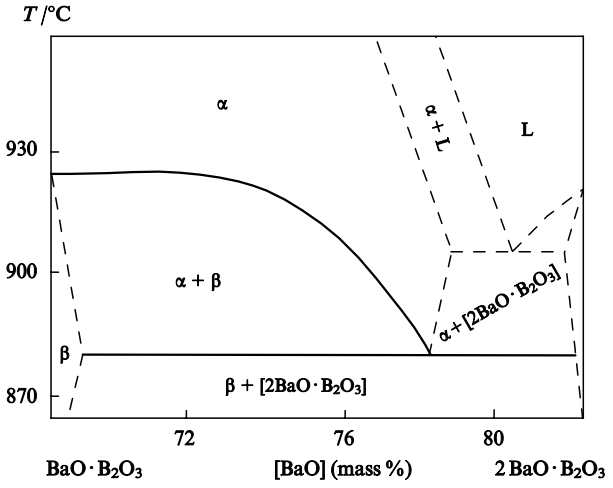


Figure 4. Middle part of the phase diagram of the $BaO - B_2O_3$ system.[62]

version of the phase diagram, the low-temperature modification of β-BaB_2O_4 is not in the equilibrium with the B_2O_3-enriched melt; however, this contradicts the results obtained more recently.[63, 64]

Hübner [65] also studied the phase equilibria in the $BaO - B_2O_3 - Al_2O_3$ system and reported the formation of continuous solid solutions in the composition range between $2\,BaO \cdot B_2O_3$ and the low-temperature modification of $BaO \cdot B_2O_3$ at 700 °C (Fig. 5). The formation of individual compound $2\,BaO \cdot B_2O_3$ was established based on the X-ray diffraction data obtained in melt crystallisation studies in a number of ternary systems.[66] Compound $2\,BaO \cdot B_2O_3$ crystallises in the monoclinic crystal system (Table 1) and its unit cell parameters are close to those of β-BaB_2O_4 in the monoclinic setting (the difference consists in doubling the parameter *c*). This structural type is possible only if barium and oxygen ions are inserted into the β-BaB_2O_4 lattice, which is accompanied by a dramatic increase in density.

Single crystals of the $2\,BaO \cdot 5\,B_2O_3$ ($Ba_2B_{10}O_{17}$) phase found by Hübner [62] were grown by Stone *et al.*[68] by slowly cooling a stoichiometric melt. The solid-phase synthesis was carried out at 750 °C and the melting temperature of the compound was reported to be 901 °C. The melt undergoes a glass transition on cooling with ease.

The crystal structures of compounds $BaO \cdot 2\,B_2O_3$ (BaB_4O_7), $BaO \cdot 4\,B_2O_3$ (BaB_8O_{13}) and $2\,BaO \cdot 5\,B_2O_3$ ($Ba_2B_{10}O_{17}$) were established (see Table 1).[16, 18, 68] At 700 °C, compound $BaO \cdot 4\,B_2O_3$ undergoes a phase transition from the low-temperature orthorhombic to the high-temperature tetragonal modification which is stable up to the congruent melting temperature (889 °C).[67] The heat of the transition is 2100 J mol^{-1}. The phase transition is accompanied by twinning of crystals.

An IR spectroscopic study [75] revealed the presence of isolated BO_3 triangles in the structure of compound $3\,BaO \cdot B_2O_3$ which is thus an orthoborate.

The generalised phase diagram of the $BaO - B_2O_3$ system is shown in Fig. 6. Since the melting temperature of compound $Ba_2B_{10}O_{17}$ (see Ref. 68) is somewhat higher than the liquidus temperature for this composition (see Ref. 12), this compound seems to be stable. According to the version of the phase diagram proposed by Levin and McMurdie,[12] an eutectic corresponding to the crystallisation of $BaO \cdot 2\,B_2O_3$ and $BaO \cdot 4\,B_2O_3$ should occur in this concentration range; however, no eutectic effects were observed. Probably, they simply overlooked the compound $2\,BaO \cdot 5\,B_2O_3$. Earlier,[60] a congruently melting compound of other stoichiometric composition was found in this concentration range.

The 'interrelation' between compounds $2\,BaO \cdot B_2O_3$ and $BaO \cdot B_2O_3$ is still a moot question. The melting temperature of $2\,BaO \cdot B_2O_3$ reported by Hübner is much lower than the liquidus

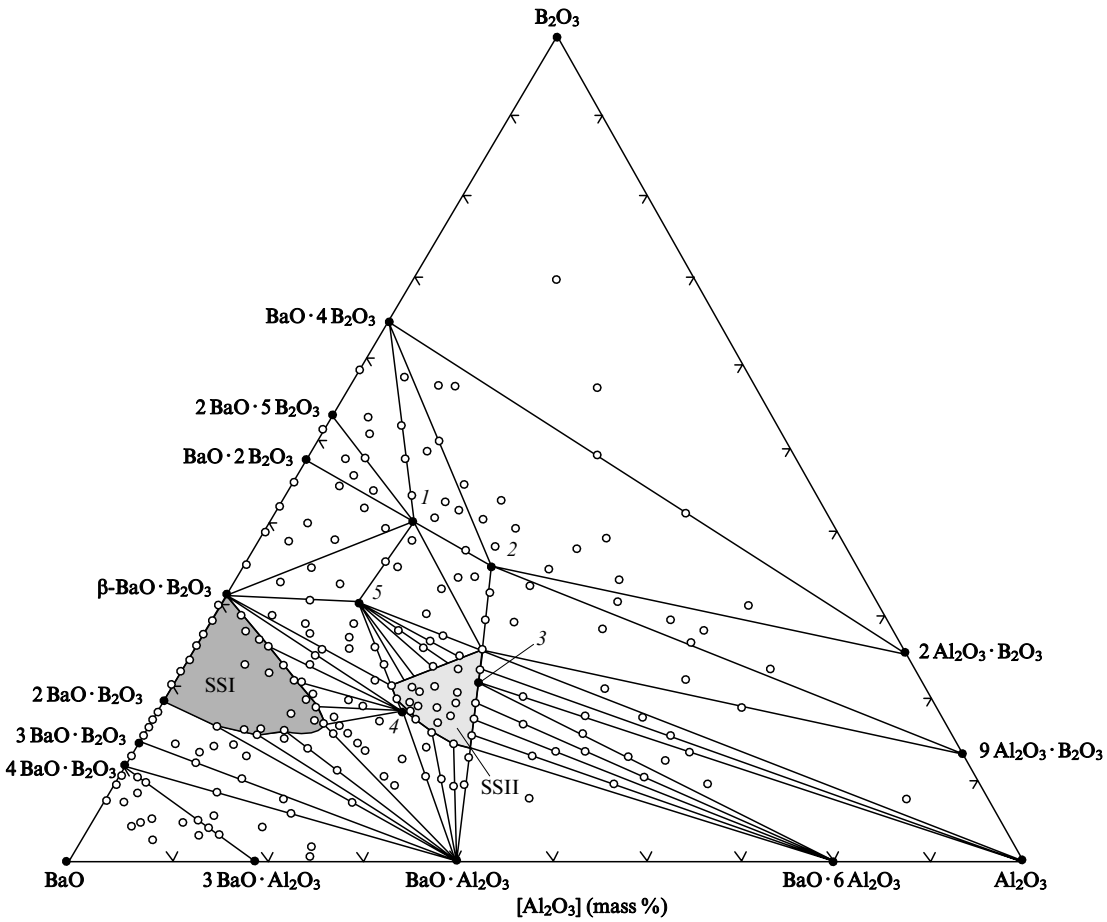


Figure 5. Phase equilibria in the $BaO-B_2O_3-Al_2O_3$ system at 700 °C.[65]
Open circles denote the compositions studied; full circles denote compounds; SSI and SSII designate the regions of solid solutions; $2\,BaO\cdot 4\,B_2O_3\cdot Al_2O_3$ (*1*), $BaO\cdot 2\,B_2O_3\cdot Al_2O_3$ (*2*), $BaO\cdot B_2O_3\cdot Al_2O_3$ (*3*), $3\,BaO\cdot 2\,B_2O_3\cdot 2\,Al_2O_3$ (*4*) and $5\,BaO\cdot 6\,B_2O_3\cdot 2\,Al_2O_3$ (*5*).

Table 1. Crystallographic characteristics of anhydrous barium borates.

Compound	Crystal system	Space group	Unit cell parameters					Density /g cm^{-3}	Ref.
			a /Å	*b* /Å	*c* /Å	α, β, γ /deg	*Z*		
$BaB_{8\frac{1}{3}}$	orthorhombic	$P222_1$	8.56	17.38	13.20		8	2.91	18
			8.55	17.352	13.21		8	2.927	67
	tetragonal [a]		8.630		13.268		4	2.899	67
BaB_{47}	monoclinic	$P2_1/c$	10.56(1)	8.20(1)	13.01(1)	$\beta = 104.95(17)$	8	3.57	16
$Ba_2B_{10\frac{1}{7}}$	triclinic	$P1$	9.858(1)	9.990(1)	6.706(1)	$\alpha = 96.79(1)$ $\beta = 106.64(1)$ $\gamma = 76.89(1)$	2	3.54	68
β-BaB_{24}	trigonal	$R3c$	12.532		12.717		18	3.74	22
			12.529		12.731		18	–	69
			12.519		12.723		18	–	70
			12.547(6)		12.736(9)		18	–	44
			12.500(3)		12.6875(9)		18	–	71
			12.517(3) [b]		12.708(3) [b]		18	–	72
α-BaB_{24}	trigonal	$R\bar{3}c$	7.2188(10)		39.000(4)		18	3.734	17
			7.2351		39.192		18	3.751	73
Ba_2B_{25}	monoclinic	$P2$, Pm or $P2/m$	11.014(6)	12.684(5)	16.856(7)	$\beta = 99.82(3)$	19	5.07	62
	trigonal	–	21.70 [c]		12.74 [c]				
Ba_3B_{26}	orthorhombic	–	13.82	14.81	13.43		16	5.11	74

[a] At 725 °C. [b] Doped with neodymium. [c] Recalculated by the authors of this review using Hübner's data.[62]

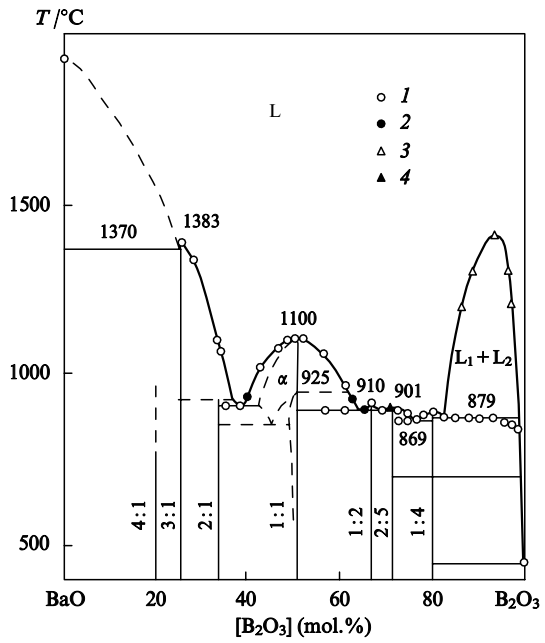


Figure 6. Generalised phase diagram of the $BaO-B_2O_3$ system. The data were taken from Ref. 12 (*1*), Ref. 64 (*2*), Ref. 61 (*3*) and Ref. 68 (*4*).

temperatures determined earlier [12, 59] and, hence, cannot correspond to the equilibrium congruent melting of this compound. However, it is rather close to the eutectic temperature. The authors of this review suggest incongruent melting of $2\,BaO\cdot B_2O_3$ following a peritectic reaction (see Fig. 6).

Hübner's assumption [62] of the presence of the homogeneity region based on $BaO\cdot B_2O_3$ is in agreement with the absence of eutectic effect in this concentration range.[12] Figure 6 presents a version of the phase diagram containing the regions of solid solutions based on α-BaB_2O_4 and β-BaB_2O_4 shown according to Hübner. The presence of these regions suggests a strong nonstoichiometry of BaB_2O_4. If this is the case, the maximum on the liquidus curve should not coincide with the point corresponding to the 1 : 1 composition. It should also be noted that the densities of both the α- and β-modifications of BaB_2O_4 are much lower than the average density obtained by linear approximation of the data for compounds in the $BaO-B_2O_3$ system. This anomaly can be to some extent compensated for by the formation of interstitial solid solutions. This issue as well as the thermal stability of $4\,BaO\cdot B_2O_3$ call for further investigation.

III. Glass formation in the $BaO-B_2O_3$ system

Melt cooling in the $BaO-B_2O_3$ system causes glass formation.[9, 11, 14] The most stable glasses (ingots up to 50 g by mass) are fabricated by solidification of melts containing from 16 mol.% to 40 mol.% BaO, *i.e.*, in the region of existence of the low-melting compounds $BaO\cdot 2\,B_2O_3$, $2\,BaO\cdot 5\,B_2O_3$ and $BaO\cdot 4\,B_2O_3$ (see Fig. 6). As the cooling rate increases, the region of glass formation extends (up to 60.5 mol.% BaO for ingots of mass 0.1 g) and includes the composition BaB_2O_4. No transparent homogeneous glasses are formed on cooling of B_2O_3-enriched melts. At temperatures that are somewhat higher than the liquidus temperature, the equilibrium melt represents two immiscible liquids of different compositions. Similarly to the melt, on cooling each of the liquids can undergo a glass transition.

Boron oxide can undergo a spontaneous glass transition.[9] Glassy boron oxide can be readily obtained from boracic acid which melts at 176 °C. Long-term heating is accompanied by slow removal of water from the melt; however, trace amounts of water are hard to remove. The content of the residual water after heating at 1200 °C for 19 h is 0.127 mass %. Pumping anhydrous dinitrogen through the melt over a period of 5 h reduces the content of water down to 0.025 mass %. A nearly completely dehydrated material was prepared by long-term heating at a pressure of 1 Torr in a platinum crucible and then in a graphite crucible. The viscosity of the melt depends on the content of water; as this parameter decreases from 0.248 mass % down to 0.025 mass %, the temperature corresponding to a viscosity of 10^4 P increases from 537 to 550 °C.

It is noteworthy that the viscosity of B_2O_3 at 450 °C (melting temperature) is much lower than that of silica at 1710 °C; however, glassy boron oxide is much more hard to crystallise compared to glassy silica. This was assumed to be due to abnormally high ratio of the bond energy to the melting temperature of glassy B_2O_3. No spontaneous devitrification of B_2O_3 at an atmospheric pressure was observed. Crystallisation of boron oxide requires heating at 225–250 °C over a period of several days in a loosely plugged vessel. The sample slowly loses water and is transformed into a solid finely crystalline aggregate characterised by a density of 2.42 g cm^{-3} and a melting temperature lying between 460 and 470 °C. The content of B_2O_3 in the material thus obtained is 99.4% while the rest seems to be the bound water.

An X-ray study of glassy B_2O_3 showed that its structure is a disordered network of $[BO_3]^{3-}$ triangles (in which each oxygen atom is linked to two boron atoms) or distorted $[BO_4]$ tetrahedra.

Glass formation is also typical of the systems comprising B_2O_3 and alkali metal oxides. The $Na_2O-B_2O_3$ system is characterised by two glass formation regions[14] corresponding to the concentration ranges 0 mol.% – 8 mol.% (or 0 mol.% – 30 mol.%) and 66.5 mol.% – 71.5 mol.% Na_2O. The second glass formation region coincides with the region of existence of low-melting compositions in the vicinity of the $NaBO_2-Na_4B_2O_5$ eutectic. A 'belt'-like glass formation region was found in the $Na_2O-BaO-B_2O_3$ system at the B_2O_3 concentration of greater than 60 mol.%.[76]

IV. Methods of preparation of BaB_2O_4

There are four groups of methods for preparation of BaB_2O_4. These are precipitation of crystal hydrates from aqueous solutions followed by dehydration; hydrolysis of alkoxides; anhydrous solid-phase syntheses (possibly) followed by melting and melt-solution syntheses. The last-named group also includes various single-crystal growth techniques which can be considered as specific methods of synthesis.

1. Precipitation of $BaB_2O_4\cdot n\,H_2O$ from aqueous solutions

Methods for the synthesis of barium borate based on precipitation of crystal hydrates $BaB_2O_4\cdot n\,H_2O$ from aqueous solutions (aqueous methods) have been known for long.[2–8] However, they are rarely employed for the preparation of charge that is used as raw material for the crystal growth.

Aqueous methods for the synthesis of different metal borates share a number of features. During precipitation from aqueous solutions the borates are isolated as crystal hydrates. The content of the bound water depends on the reaction conditions. In addition, metal borates can be isolated in the amorphous state. Such borates are intermediate products of many syntheses; nevertheless, they can undergo a transition into the crystalline state under particular conditions. Amorphous borates are, as a rule, highly reactive.

Borates can contain water in the form of both hydroxyl ion and solvate molecules. This allows one to rationalise a complex process of dehydration of borates at elevated temperatures which involves elimination of individual solvate water molecules and hydroxyl groups, which is due to association of boron-containing anions. Usually, removal of water occurs in a stepwise manner in the temperature range from 100 to 200 °C. The residual water can be removed only at very high temperatures (~1000 °C and above). Often, dehydration of borates is accompanied by a specific

effect of borate rearrangement [77] which was first reported by Nikolaev.[78] Namely, dehydration causes a complete destruction of the crystal lattice and transition of the compound under study into the amorphous state; further heating leads to crystallisation accompanied by exothermic effect, which can be detected on thermograms.

The synthesis of BaB_2O_4 by precipitation from aqueous solutions should be carried out in a strongly basic medium (pH > 11) provided that variations of the pH value during crystallisation are small. This can be done by performing a reaction between a solution of boric acid and a solution of $Ba(OH)_2$ (see Ref. 4) or $BaCl_2$.[51] However, it is more convenient to use barium chloride and a mixture of sodium tetraborate and sodium hydroxide.

$$BaCl_2 + Na_2B_4O_7 + 2\,NaOH + 3\,H_2O = \\ = BaB_2O_4 \cdot 4\,H_2O\downarrow + 2\,NaBO_2 + 2\,NaCl.$$

To maintain the pH value at the desired level, a nearly twofold excess of the precipitating agent is required. The reaction results in a flaky precipitate which is transformed into crystalline $BaB_2O_4 \cdot 4\,H_2O$ after several hours.

The crystallisation fields of $BaB_2O_4 \cdot 4\,H_2O$ and $BaB_2O_4 \cdot 5\,H_2O$ in sodium borate solutions at 25 °C for the reaction presented above were studied by Gode.[5] The possibility of nearly complete precipitation of boron (in the form of barium borate) from solutions was demonstrated (see Fig. 2 *b*). A drawback of this method consists in poisoning the precipitate by sodium and chlorine impurities.

The synthesis of barium borate from barium nitrate was proposed [8]

$$Ba(NO_3)_2 + Na_2B_4O_7 + 2\,NaOH + 3\,H_2O = \\ = BaB_2O_4 \cdot 4H_2O\downarrow + 2\,NaBO_2 + 2\,NaNO_3.$$

It was proposed to remove the chloride (impurity in NaOH) and sodium ions using an ammonia solution (to prevent transformation into polyborates). Drying at 400–650 °C for 30 min resulted in an anhydrous product.

To transform non-crystalline barium borate into the crystalline $BaO \cdot B_2O_3 \cdot 4\,H_2O$, it was recommended [6] to grind the material in a boric acid solution in the presence of KOH. The yield of the desired product was low (~20%).

Dehydration of the tetrahydrate $BaO \cdot B_2O_3 \cdot 4\,H_2O$ begins at 70 and is completed at 140 °C, while dehydration of the pentahydrate $BaO \cdot B_2O_3 \cdot 5\,H_2$ occurs in the temperature range from 50 to 450 °C.[4] It should be noted that the melting temperatures of the dehydrated products (1015 and 925 °C, respectively) [4] are much lower than the equilibrium melting temperatures. Probably, this is due to the influence of the residual water. According to Lehmann *et al.*,[51] dehydration of $BaO \cdot B_2O_3 \cdot 1.67\,H_2O$ occurs in the temperature range 90–170 °C.

Precipitation of the tetrahydrate $BaB_2O_4 \cdot 4\,H_2O$ from solution followed by thermal decomposition following the reactions

$$BaCl_2 \cdot 2\,H_2O + 2\,H_3BO_3 = BaB_2O_4 \cdot 4\,H_2O\downarrow + 2\,HCl, \quad (1)$$

$$BaB_2O_4 \cdot 4\,H_2O = BaB_2O_4 + 4\,H_2O \quad (2)$$

was employed [79–82] for the synthesis of BaB_2O_4 that is used as raw material (charge) for the melt growth of β-BaB_2O_4 crystals (the so-called chloride technique). Remelting or sintering BaB_2O_4 at 1095 °C for 3 h results in a coarse-grained material of higher purity grade compared to the charge obtained by solid-phase synthesis from barium carbonate. A thermogram exhibiting a clearly seen peak corresponding to the melting at 1100 °C has been reported.[82]

It should be noted that the synthesis of BaB_2O_4 by thermolysis of crystal hydrates allows reliable preparation of a product of stoichiometric composition. In addition, it seems that aqueous solutions favour purification of barium-containing reagents (removal of impurities including strontium and calcium that strongly affect the stability of the crystalline modifications of BaB_2O_4).

2. Syntheses using 'soft chemistry' methods

Recently, the so-called 'soft chemistry' methods have been used for the synthesis of inorganic materials (see, *e.g.*, Ref. 83). These methods can also be employed to synthesise barium borate. For instance, a stoichiometric mixture of boron triethoxide and barium isopropoxide was slowly hydrolysed with distilled water.[84] The powder dried *in vacuo* at 60 °C was found to be a new γ-modification of BaB_2O_4.

3. Anhydrous high-temperature syntheses

Compound BaB_2O_4 can be directly synthesised by melting BaO and B_2O_3 at 1150 °C for 1 to 2 h.[85] According to the results of differential thermal analysis (DTA) study, the reaction begins at 1060 °C.

Barium borate (the starting material for the synthesis of single crystals) is usually prepared from a mixture of $BaCO_3$ and B_2O_3 (see Refs 86–89) or H_3BO_3.[64, 80, 90–92] The syntheses are conducted using the following reaction equations

$$BaCO_3 + B_2O_3 = BaB_2O_4 + CO_2\uparrow, \quad (3)$$

$$BaCO_3 + 2\,H_3BO_3 = BaB_2O_4 + 3\,H_2O\uparrow + CO_2\uparrow. \quad (4)$$

Powder mixtures taken in the stoichiometric ratios are mechanically mixed and then heated until sintering and melting. In the case of reaction (3) the powders are sintered at 800 °C for 10 h, melted at 1200 °C for 10 min and then zone melted (both processes are carried out in a graphite boat in an argon atmosphere) [88] or are melted in air at 1150 °C for 5 h. For the reaction with H_3BO_3 it was recommended [92] to use a stepwise synthesis with allowance for the reaction mixture to stay at 150 and 700 °C.

Usually, syntheses are performed in platinum crucibles; however, graphite crucibles can also be used in an inert atmosphere (argon).[88]

It seems likely that one can synthesise BBO from barium carbonate according to Berzelius by boiling a barium carbonate suspension in an aqueous boric acid (analogously to the synthesis of lead borate [4]). However, this synthetic route was not studied experimentally.

Barium borate BaB_2O_4 is also synthesised using other barium compounds (*e.g.*, barium oxide,[79] barium acetate [90, 91] and barium nitrate [12, 82]) as starting reagents.

$$BaO + 2\,H_3BO_3 = BaB_2O_4 + 3H_2O\uparrow,$$

$$Ba(CH_3COO)_2 + 2\,H_3BO_3 + 4\,O_2 = \\ = BaB_2O_4 + 6\,H_2O\uparrow + 4\,CO_2\uparrow,$$

$$Ba(NO_3)_2 + 2\,H_3BO_3 = BaB_2O_4 + N_2O_5\uparrow + 3\,H_2O\uparrow.$$

The reaction with barium acetate was carried out in a platinum crucible using stepwise heating;[91, 92] finally, the product was kept at 1150 °C for 50 h. The reaction proceeds in air; however, it does not always happen that the reaction goes to completion under the crystal growth conditions. This leads to poisoning the growing crystals with carbon. In the reaction with barium nitrate the ground mixture of reagents was heated to 700 °C for 2 h and then repeatedly heated above this temperature.[12]

The following reaction was conducted [82]

$$Ba(NO_3)_2 + B_2O_3 = \beta\text{-}BaB_2O_4 + N_2O_5\uparrow.$$

A ground mixture of reagents was repeatedly heated from 700 to 850 °C. It was also found that the reactions of $BaCO_3$ or BaO with H_3BO_3 do not result in products that are suitable for the Czochralski growth of β-BaB_2O_4.

4. Melt-solution crystallisation

Barium borate can be synthesised by exchange reactions in melts. The first successful synthesis dates back to 1874.[1,79] The following reaction was used

$$BaCl_2 + 2\,NaBO_2 = BaB_2O_4\downarrow + 2\,NaCl.$$

Sodium chloride having a lower melting temperature acts as solvent that is removed with water after cooling.

Reactions analogous to the processes underlying the aqueous methods of synthesis[93,94] can also be used for the synthesis of β-BaB_2O_4

$$BaCl_2 + B_2O_3 \xrightarrow{H_2O} BaB_2O_4\downarrow + 2\,HCl\uparrow,$$

$$BaCl_2 + 2\,H_3BO_3 = BaB_2O_4\downarrow + 2\,HCl\uparrow + 2\,H_2O\uparrow.$$

The excess barium chloride acts as flux. The reaction was carried out in a platinum crucible at 1000 °C for 2 h.[93] The driving force of the synthesis of BaB_2O_4 is the difference between the heat of reaction and the energy of pyrohydrolysis of barium chloride (~78 kcal).

A method of fabrication of a seed rod necessary for melt-solution growth of single crystals is as follows.[94] BaB_2O_4 polycrystals precipitated in the reaction with boric acid are ground, moulded, sintered in an oxygen atmosphere at 730–850 °C, reground and then re-sintered at 850–1095 °C.

An extensive literature on the synthesis of single crystals using the systems of the BaB_2O_4–S or, more generally, $BaO-B_2O_3$–S types (S is the melt playing the role of solvent) has evolved. Both equilibrium and nonequilibrium melt crystallisations are possible (the former corresponding to the primary crystallisation region of β-BaB_2O_4 in the phase diagrams). Among various solvents, Na_2O is most widely used at present (see below).

Melt-solution growth of single crystals is strongly affected by the impurities coming into the crystal from the solvent. These are the melt components (first of all, sodium), impurities contained in the starting reagents and accumulated within the growing crystal (*e.g.*, potassium or strontium) and 'extra' impurities that come from the material the crucible is made of (platinum).

V. Polymorphism and the crystal structure

In addition to the high- and low-temperature modifications of BaB_2O_4 (these two were mentioned above) there are some indications of the existence of at least one unstable low-temperature modification designated as T-BaB_2O_4 (see Ref. 51), or γ-BaB_2O_4.[84,95] The X-ray diffraction patterns of the samples reported in Refs 51, 84 and 95 are close but not identical. The samples of this phase were obtained by dehydration of $BaB_2O_4\cdot 1.67\,H_2O$ (see Ref. 51) and by the interaction of boron triethoxide and barium isopropoxide. According to Yamaguchi *et al.*,[84] γ-BaB_2O_4 undergoes an irreversible transformation into α-BaB_2O_4 on heating to ~600 °C. An IR spectroscopic study of γ-BaB_2O_4 showed that, in contrast to the structure of the α- and β-forms of BaB_2O_4 (see below), the structure of this modification comprises infinite anionic chains constructed of $[BO_4]$ tetrahedra with their vertices shared (calcium, strontium and lithium metaborates have an analogous structure).¶

The crystal structure of α-BaB_2O_4 was established by Mighell and Perloff.[17] It was found that the crystal is characterised by the trigonal system and centrosymmetric space group $R\bar{3}c$ (Fig. 7).

According to Hübner,[62] β-BaB_2O_4 single crystals have a monoclinic unit cell with the parameters $a = 11.133$, $b = 12.67$, $c = 8.381$ Å and $\beta = 100.04°$; the space group is $C2/c$ and $Z = 12$. Coincidence of the results of X-ray powder diffraction studies[12,62] indicates that the same modification of barium borate was investigated in both cases.

However, Hübner's[62] choice of the unit cell was questioned.[69] According to Liebertz and Stahr,[69] β-BaB_2O_4 crystals are uniaxial and trigonal (the crystallographic parameters are listed in Table 1). This discrepancy is of fundamental nature, since the space group $C2/c$ is centrosymmetric while the space group $R3c$ is non-centrosymmetric. Frohlich[70] established the crystal structure of β-BaB_2O_4 and confirmed the results obtained by Liebertz and Stahr.[69] Lu *et al.*[22] also reported similar results; however, they believed that the β-BaB_2O_4 crystal is characterised by the space group $R3$. The results obtained by Lu *et al.*[22] were used in the interpretation of the Raman spectra of β-BaB_2O_4 crystals.[97] Redetermination of the crystal structure[44,71] and the results of piezoelectric and electro-optical measurements[38,98] and Raman spectroscopy studies[99,100] confirmed that the low-temperature modification of barium borate is characterised by the space group $R3c$.

A thorough study[85] of BaB_2O_4 single crystals confirmed the lack of central symmetry and revealed a slight monoclinic distortion of the trigonal lattice. The parameters of the trigonal lattice of β-BaB_2O_4 obtained by different authors are slightly different (see Table 1).

The high- and low-temperature modifications of barium borate exhibit pronounced structural similarity, *viz.*, both of them have layered structures, contain nearly planar boron–oxygen $[B_3O_6]^{3-}$ ring groups arranged perpendicular to the three-fold axis while their lattice parameters are related by simple formulae $a_\alpha \approx \sqrt{3}a_\beta$, $c_\alpha \approx (1/3)\,c_\beta$, $Z_\alpha = Z_\beta$.

The $[B_3O_6]^{3-}$ groups are constituents of the structure of only one out of the three known crystalline modifications of metaboric acid, namely, metastable orthorhombic HBO_2-III with a melting temperature of 176 °C.[3] Therefore, the α- and β-modifications of BaB_2O_4 are salts of this acid.

High-temperature Raman spectroscopy studies[99,100] of the α- and β-forms of BaB_2O_4 revealed a change in the number of spectral lines in the frequency range of internal vibrations of the $[B_3O_6]^{3-}$ anions corresponding to the D^6_{3h} and C^6_{3v} symmetry, respectively. The B–O distances in and out of the ring are ~1.40 and 1.32 Å, respectively.

The structures of the α- and β-modifications of BaB_2O_4 are characterised by different types of coordination environment of barium ions. In the high-temperature α-modification there are two types of barium atoms. The coordination number of barium atoms occupying the first position is 6 while for Ba atoms in the second position it equals 9. In the low-temperature β-modification the Ba atoms are in irregular environment of eight oxygen atoms shared by three ring borate anions. The Ba–O distances, d(Ba–O), lie between 2.613 and 3.025 Å. The X-ray powder diffraction patterns of the α- and β-modifications of BaB_2O_4 are presented in Fig. 8.

Investigation of the nonlinear optical properties of BBO is a topical problem. In this connection it is appropriate to briefly outline the nature of chemical bonding in this compound.[38,40–43,97] In the $[B_3O_6]^{3-}$ ring anions, the sp^2-hybridised boron atoms form σ-bonds with oxygen atoms. The filled orbitals of the oxygen atoms and the vacant orbitals of the boron atoms involved in the rings interact with one another, thus forming the π-bonds. Positively charged Ba^{2+} ions and negatively charged $[B_3O_6]^{3-}$ groups interact electrostatically. In addition, the intermolecular interaction occurs between electrically neutral layers. A number of the first-principle studies of the electronic structure and nonlinear optical susceptibilities of BBO have been reported.[42,43] The results of calculations are in good agreement with the experimental data. The energy states of the atoms constituting the $[B_3O_6]^{3-}$ anions contribute to both the upper part and the bottom of the conduction band.

Different temperatures of the phase transition between the β- and α-modifications of BaB_2O_4 have been reported (100–400 °C,[12] 880 °C,[103] ~900 °C [44] and 917 °C [104]). Currently, a value of 925±5 °C reported by Hübner[62] and confirmed

¶ In addition, two unstable modifications of BaB_2O_4 were obtained during crystallisation of glasses in the $BaO-B_2O_3-Al_2O_3$ system.[65]

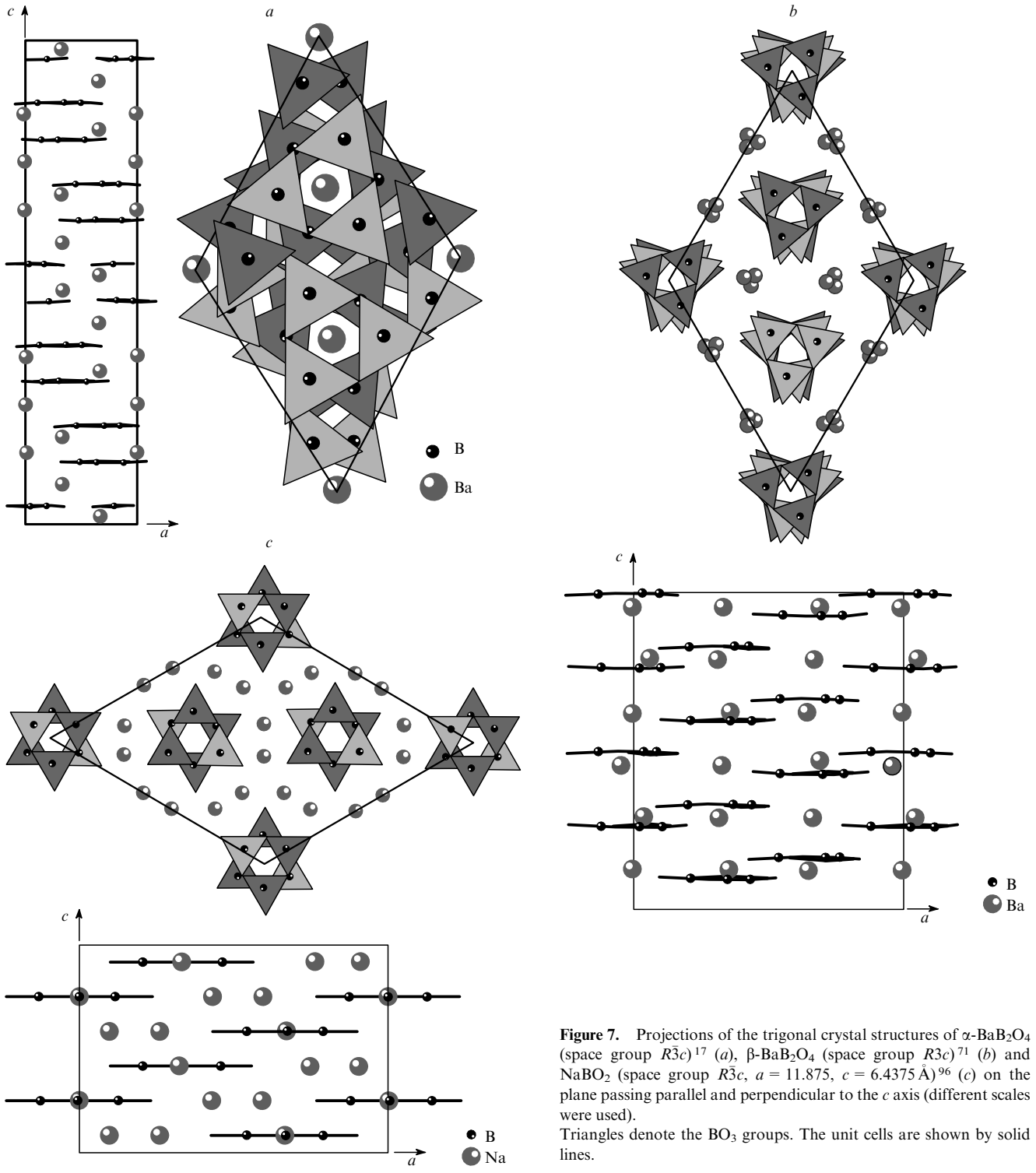


Figure 7. Projections of the trigonal crystal structures of α-BaB_2O_4 (space group $R\bar{3}c$)[17] (*a*), β-BaB_2O_4 (space group $R3c$)[71] (*b*) and $NaBO_2$ (space group $R\bar{3}c$, $a = 11.875$, $c = 6.4375$ Å)[96] (*c*) on the plane passing parallel and perpendicular to the *c* axis (different scales were used).
Triangles denote the BO_3 groups. The unit cells are shown by solid lines.

in the annealing and quenching studies[23, 105] has been commonly accepted.

The phase transition in question is strongly hindered. An X-ray diffraction pattern obtained after annealing of coarse-grained (40–50 μm), single-phase (β-phase) crystalline BBO at 940 °C for 4 h exhibited only traces of the α-phase.[87] Annealing at higher temperatures is accompanied by gradual decrease in the intensity of the reflections of the β-phase and by simultaneous increase in the intensity of the reflections of the α-phase. After annealing at 960 °C for 2 h nearly ∼50% of the initial β-phase transformed into the α-phase. Analogous studies were carried out using single-phase (α-phase) crystalline BBO. After annealing at ∼800 °C for 7 h nearly ∼30% of the initial α-phase transformed into the β-phase. At lower temperatures, the phase transformation occurred very slowly.

During measurements[106] of the thermal expansion coefficients the BBO single crystals were overheated up to 983 °C at a heating rate of 1 deg min^{-1} and to 1010 °C at a heating rate of 0.1 deg min^{-1}. Transition into the α-phase occurred after reaching these temperatures.

According to Kimura and Feigelson,[107] the β → α transformation takes only 5 min on heating above 1000 °C. It should be noted that the samples studied contained Sr (∼0.05%) and Ca (∼0.03%); it is thought that Ca impurity causes stabilisation of the α-phase.[108]

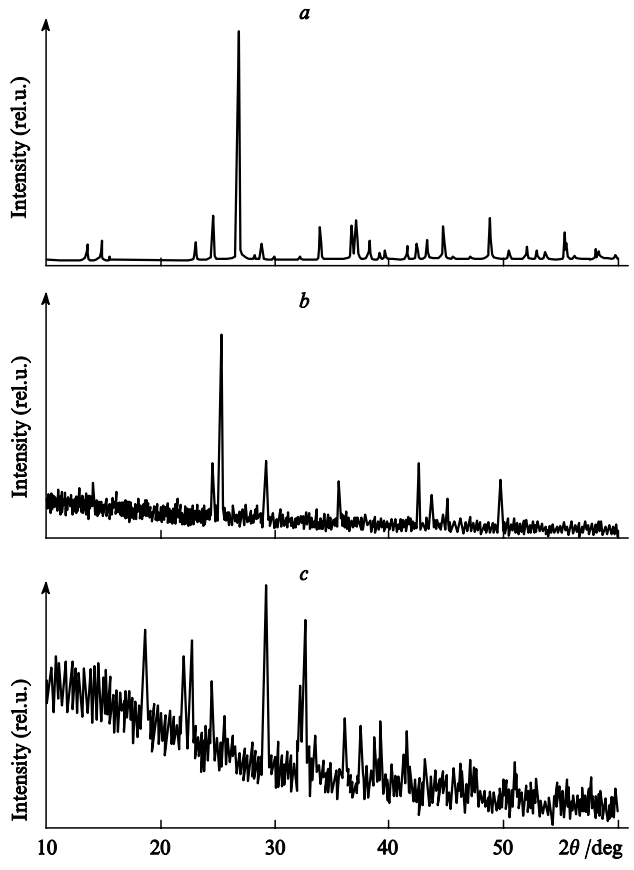


Figure 8. X-Ray powder diffraction patterns (CuK_α radiation) of α-BaB_2O_4 (*a*), β-BaB_2O_4 (*b*) and $NaBaBO_3$ (*c*).[101, 102]

A number of *in situ* studies of the β ⇄ α transformation by high-temperature X-ray powder diffraction have been reported.[82, 84, 106] Kozuki and Itoh[106] heated BBO powder to 1050 °C but no phase transition was observed. Yoshimoto and Kimura[82] also did not observe the β → α and α → β phase transitions upon heating to 1000 °C. According to Yamaguchi *et al.*,[84] transformation of β-BaB_2O_4 prepared by heating from the γ-modification into α-BaB_2O_4 begins at 870 °C and is completed at 940 °C. The kinetics of this transformation have been studied.

The most surprising results were reported by Kouta *et al.*[80] who studied the transition in question and did not observe even minor indications of the phase transformation after heating β-BaB_2O_4 powder at 1090 °C for 5 h and subsequent cooling of the sample. The results of DTA study[80] showed that both modifications of BaB_2O_4 melt at nearly the same temperature, namely, 1100 ± 0.5 °C (α-phase) and 1099 ± 0.5 °C (β-phase).

A special study concerning the influence of the heating and cooling rates (υ = 3.75, 5.0, 7.5, 10.0, 15.0 deg min^{-1}) on both the transition temperatures and reversibility of the phase transformations has been reported.[104] It was shown that the temperatures of the polymorphic transition of the low-temperature modification of BaB_2O_4 into the high-temperature form (917 °C) and the melting temperature of the latter (1092 °C) are virtually independent of the heating rate, whereas the reverse is observed on cooling.

VI. Peculiarities of crystallisation of BaB_2O_4 melts

BBO melts are characterised by high viscosity, tendency to supercooling and by hysteresis of properties. The physical properties of BBO have been studied recentlly.[81, 109] The viscosity of the melt monotonicaly increases from 20 to 61 mPa cm^{-1} as the temperature decreases from 1463 to 1271 K and is ~30 mPa cm^{-1} at the melting temperature. The activation energy of the viscous flow for the melt is 0.95 eV. The time taken to achieve the equilibrium viscosity of the melt at 1463 K is nearly 10 h. The density of the melt is a linear function of the temperature in the range between 1463 and 1271 K; it is described by the following equation

$$\rho = (4.453 - 0.000545)T$$

It was found that ρ = 3.707 g cm^{-3} at the melting temperature. The thermal expansion coefficient of the melt is 1.5×10^{-4} K^{-1}. The surface tension at the melting temperature is 0.35 N m^{-1} (see Ref. 89).

According to the results of our experiments data and to Itoh *et al.*[79], the degree of supercooling of the melt (ΔT) in a platinum crucible can be as high as 250 °C at cooling rates spanning the range from 4 to 15 deg min^{-1}. In this case crystallisation of β-BaB_2O_4 can occur at temperatures that are much higher than the temperature of the polymorphic transition. Crystallisation occurs randomly; there is a wide spread of the melt crystallisation temperature values but no correlations between this temperature and the cooling rate are observed. Mention has been made that the degree of supercooling of the melt can be as high as 300 °C.[110] The problem of crystallisation of BBO (spontaneous crystallisation, seed crystallisation using α-BaB_2O_4 and β-BaB_2O_4 and crystallisation on a platinum wire) has been the subject of numerous studies.

In a study[104] the degree of supercooling of the melt was 170–200 °C. On cooling (υ = 3.75, 5.0, 7.5, 10.0, 15.0 deg min^{-1}), crystallisation occurred only at the temperature of the polymorphic transition or at lower temperatures and resulted in the low-temperature modification of BaB_2O_4. The crystallisation temperatures were found to be T_c = 917 °C at υ = 3.75 and 5 deg min^{-1}, T_c = 887 °C at υ = 7.5 deg min^{-1} and T_c = 857 °C at υ = 15 deg min^{-1}.

BBO melts can exist without any changes in the metastable state for long at temperatures that are higher than the temperature of the polymorphic transition and lower than the melting temperature. However, seeding causes rapid crystallisation the rate of which increases with temperature. If α-BaB_2O_4 is used as seed, the same modification of barium borate crystallises. Seeding with β-BaB_2O_4 causes crystallisation of the β-modification despite its instability under these conditions.

Experiments on platinum seeded crystal growth showed[87] that co-crystallisation of β-BaB_2O_4 and α-BaB_2O_4 begins if $\Delta T \geqslant 40$ °C. At smaller ΔT values, crystallisation of the α-phase occurs, whereas β-BaB_2O_4 mainly crystallises at temperatures below 1030 °C (*i.e.*, at $\Delta T \geqslant 70$ °C).[82]

The degree of supercooling achievable using graphite crucibles is substantially lower compared to platinum crucibles; in addition, crystallisation of both the α- and β-modifications of BaB_2O_4 in graphite crucibles is possible.[107] This is thought to be due to some similarity between the trigonal structures of graphite and BBO.

Thermodynamically, the possibility of direct melt crystallisation of the low-temperature phase can be rationalised by taking into account strong supercooling of the melt and the existence of the temperature of metastable melting of the low-temperature phase (at this temperature the curves of the temperature dependences of the Gibbs thermodynamic potentials of the low-temperature phase and the melt intersect). The corresponding scheme is presented in Fig. 9. The temperature of metastable melting, T_β, of the low-temperature modification lies between the temperature of equilibrium melting, T_α, of the high-temperature modification and the temperature of polymorphic transformation, T_t. For the crystallisation of the β-phase to begin the melt temperature should be lower than T_β.

Ignoring the difference between the heat capacities of the α- and β-modifications of BaB_2O_4, the following relationship is valid:[110]

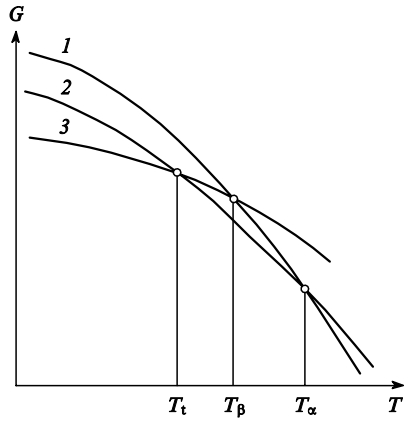


Figure 9. Temperature dependences of the Gibbs thermodynamic potentials (G) of the melt (*1*) and of the α- (*2*) and β-modifications (*3*) of BaB_2O_4.[106]
T_t is the temperature of polymorphic transformation, T_β is the temperature of metastable melting of the low-temperature modification and T_α is the temperature of the equilibrium melting of the high-temperature modification.

$$T_\beta = \frac{\Delta H_t + \Delta H_\alpha}{\Delta S_t + \Delta S_\alpha} = \frac{\Delta H_\beta}{\Delta S_\beta},$$

where ΔH and ΔS are the enthalpies and entropies of the reactions. By denoting

$$\delta = \frac{\Delta H_t}{\Delta H_\alpha},$$

one gets[111]

$$T_\beta = \frac{(\delta + 1) T_\alpha T_t}{\delta T_\alpha + T_t}.$$

The estimates of the T_β value are strongly different (Table 2).

From the standpoint of polymorphism, BaB_2O_4 presents a unique phenomenon, since both modifications (α and β) of this compound have virtually equal melting enthalpies and melting temperatures, while the enthalpy (and, correspondingly, entropy) of the α ⇄ β transition is very low.[80,82] On the other hand, here we deal with the first-order phase transition characterised by significantly different crystal structures, volumes and densities (in the temperature range from 20 to 1000 °C) of both phases. In this case, a correct thermodynamic description of the phase transformations requires that the heat capacities be taken into account (they must be measured) and, hence, the approximate relationships listed above cannot be used. Under the conditions in question the mutual stability of the polymorphous modifications strongly depends on the presence of impurities, defects, as well as on the mechanical strain and surface energy, so that the possibility of melt crystallisation of a particular modification is first of all determined by the kinetic considerations.

Table 2. Melting temperatures (°C) and enthalpies (kJ mol^{-1}) of the α- and β-modifications of BaB_2O_4.

T_α	T_β	ΔH_α	ΔH_β	Ref.
1095	1078	67.784	74.562	111
1100	1050	–	–	106
1100 ± 0.5	1099 ± 0.5	–	–	80
–	–	109.45	110.00	82

Hindered melt crystallisation of BBO can be rationalised based on structural considerations. The results of high-temperature Raman spectroscopy studies[99,100,112] of barium borate point to a dramatic difference between the spectra of the melt and crystalline β-BaB_2O_4. The spectrum of supercooled melt exhibited not only narrow lines of $[B_3O_6]^{3-}$ anions, but also a number of broad bands corresponding to internal vibrations of long-chain $[BO_2]_n^{n-}$ anions. The contribution of the $[B_3O_6]^{3-}$ anions near the melting temperature is small; however, it increases as the degree of supercooling of the melt increases. Probably, melting of BBO is accompanied by rearrangement of the boron–oxygen complexes (transformation of the $[B_3O_6]^{3-}$ ring anions into long anionic chains). Crystallisation is accompanied by the reverse rearrangement.

High viscosity of barium borate melts and their tendency to glass formation are due to the presence of long anionic chains. The hysteresis of viscosity (see above)[81,109] seems to be associated with polymerisation–depolymerisation of $[B_3O_6]^{3-}$ anions.

Structural rearrangement of the melt on heating was studied experimentally (by X-ray powder diffraction) and theoretically (by the molecular dynamics method).[113,114]

It was found[82] that self-melt crystallisation of β-BaB_2O_4 single crystals is possible if the starting material used for the preparation of the melt corresponded to the β-phase and no melt overheating occurred. The character of crystallisation of the melt can be affected by the presence of fine particles and structural fragments of crystalline phases that play the role of nucleation and crystallisation centres.[87] Overheating causes destruction of these centres. Graphite particles present in the melt can also play the role of crystallisation centres.[107]

Information on the influence of atmosphere on the character of crystallisation of BBO melts was questioned by some authors. However, an increase in the degree of supercooling of the melt in the case of crystallisation in an argon atmosphere compared to the crystallisation in air has been reported recently.[115]

VII. Growth of β-BaB_2O_4 single crystals

Peculiarities of crystallisation of BBO melts determine two most widely used methods for the growth of β-BaB_2O_4 single crystals. These are the supercooled self-melt growth (under nonequilibrium conditions) and melt-solution growth techniques. In the latter case, both single crystal growth from the equilibrium primary crystallisation region and nonequilibrium crystallisation are possible. The schemes of a number of most widely used single crystal growth techniques are presented in Fig. 10.

1. Self-melt growth of single crystals

Self-melt growth techniques of β-BaB_2O_4 single crystals have the advantages that the growing crystals are not poisoned with flux and the crystallisation rates are high (by an order of magnitude higher compared to melt-solution crystal growth). However, in these cases crystallisation occurs under nonequilibrium conditions at large temperature gradients, which causes development of mechanical strain in and cracking of the crystal. In addition, the crystal quality strongly depends on the procedure employed for the preparation of the starting reagents and on the crystallisation conditions. These methods have not received wide application so far.

Single crystals of β-BaB_2O_4 were Czochralski grown using a platinum wire seed.[79,80] Noteworthy is that only the α-modification was melt crystallised if the starting reagents were prepared by the carbonate technique [see reactions (3) and (4)]. The process using the starting reagents synthesised by the chloride method [see reactions (1) and (2)] led to direct crystallisation of the β-phase in a narrow range of the temperature gradient (G) values at the crystallisation front (G = 150–125 deg cm^{-1}). Variation of G (an increase up to 175 deg cm^{-1} and a decrease down to 50 deg cm^{-1}) resulted in the crystallisation of the α-phase. A cracked single-crystal boule 7 mm in diameter and 18 mm

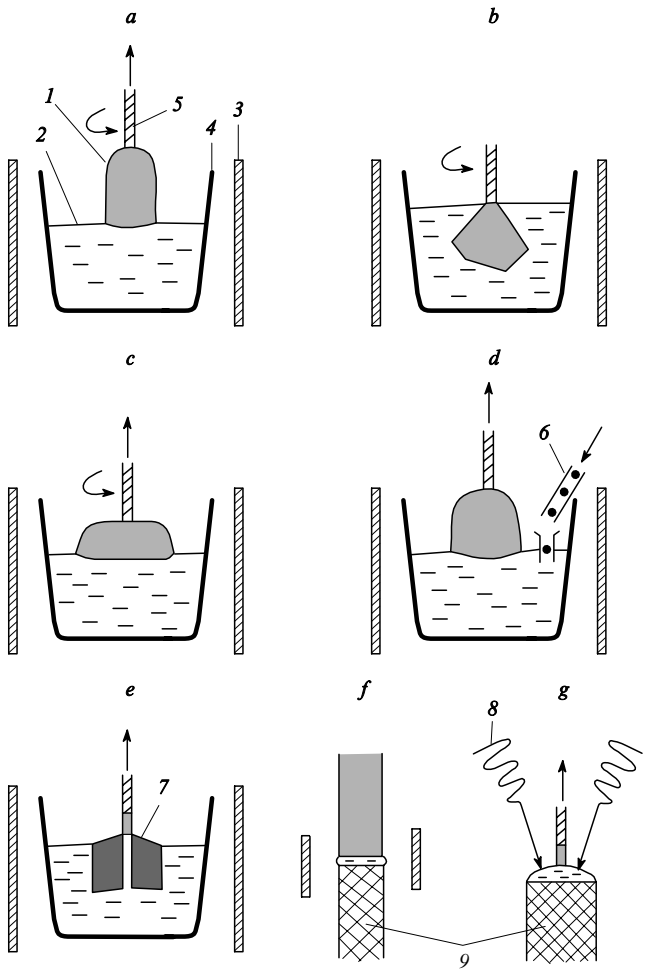


Figure 10. Schematical illustrations of the most widely used experimental techniques for the melt and melt-solution growth of single crystals.
Czochralski technique, T = const (*a*); Kyropoulos technique (immersion-seeded solution growth, ISSG), T decreases (*b*); top-seeded solution growth (TSSG) technique, T decreases (*c*); melt feed Czochralski technique (*d*); Stepanov technique, T = const (*e*); zone melting technique (*f*) and laser assisted pulling from pedestal (*g*).
Crystal (*1*); melt (*2*); heater (*3*); crucible (*4*); seed (*5*); feeding charge (*6*); shape-forming element (*7*); laser heating (*8*) and polycrystal (*9*).

long was obtained at a seed rotation rate of 20 rpm and a pulling speed of 0.6 mm h^{-1}.[79] Improvement of the growth technique allowed obtaining single crystals 15 mm in diameter and 40 mm long without cracks at a seed rotation rate of 14 rpm and a pulling speed of 4 mm h^{-1}.[80]

According to Kozuki and Itoh,[106] the upper critical temperature for stable Czochralski self-melt growth of β-BaB_2O_4 crystals is 1050 °C. The starting material (charge) is prepared from barium nitrate and boron oxide. A single crystal 15 mm in diameter and 7 mm long was grown at a seed rotation rate of 10 rpm and a pulling speed of 3 mm h^{-1}. The vertical temperature gradient was only 10 deg cm^{-1}; however, a strong influence of the radial temperature gradient was revealed (in this case, the optimum value was 77 deg cm^{-1}, see Ref. 116).

Yet another example of the Czochralski growth of β-BaB_2O_4 crystals has been reported.[89] A β-BaB_2O_4 seed of specified orientation was placed in a platinum pipe 2 or 4 mm in diameter. The charge was prepared from barium carbonate. The predominant impurity was platinum (30 ppm). The temperature gradient was 300 deg cm^{-1}. Crystals 7 mm in diameter and 20 mm long were grown at a seed rotation rate of 15 rpm and a pulling speed of 5 mm h^{-1}. The same technique was also used for the crystallisation of solid solutions β-$Ba(B_{1-x}R_x)_2O_4$ (R = Al, Ga, $0 \leqslant x \leqslant 0.1$).[116]

2. Melt-solution growth of single crystals †

a. Choice of solvent

An appropriate solvent (flux) must provide a rather extended primary crystallisation region of the low-temperature modification of BaB_2O_4 and reduce the viscosity and glass-forming ability of the melt. As a consequence, the melts should exhibit a lower degree of polymerisation of the boron–oxygen chains and an increased proportion of the $[B_3O_6]^{3-}$ ring anions. The solvent must be of low volatility, possess stable properties and provide very weak interaction with the crystal to exclude the possibility of poisoning. The melt should also not be an aggressive medium towards the material the crucible is made of.

A melt growth technique of β-BaB_2O_4 single crystals from the starting reagents using a shift from the stoichiometric composition towards an excess of BaO or B_2O_3 (the so-called self-flux) has been reported.[63,103] However, the temperature ranges suitable for crystal growth in this manner are narrow (less than 20 °C). More often, an excess of B_2O_3 is used;[120,121] however, in this case the crystal growth is hampered due to high viscosity of the melt.

A large number of compounds and their combinations have been considered as candidates for solvents. These are, *e.g.*, Li_2O,[62,103] $BaCl_2$,[103,121] BaF_2,[66,103,121,122] NaF,[66,90,91,123] LiF,[66] NaCl,[66,124–126] NaCl–Na_2O,[125] PbO,[127] Na_2O–Nd_2O_3,[72,120] $LiNbO_3$,[120] PbF_2–B_2O_3,[120] CaF_2[124] and Na_2SO_4.[124]

Usually, the solvent is chosen based on the phase diagrams of corresponding systems. Some known regions of the phase diagrams are presented in Fig. 11. The BaB_2O_4–NaCl, BaB_2O_4–

† For basic principles of the methods for melt-solution (flux) crystal growth, see Refs 117–119.

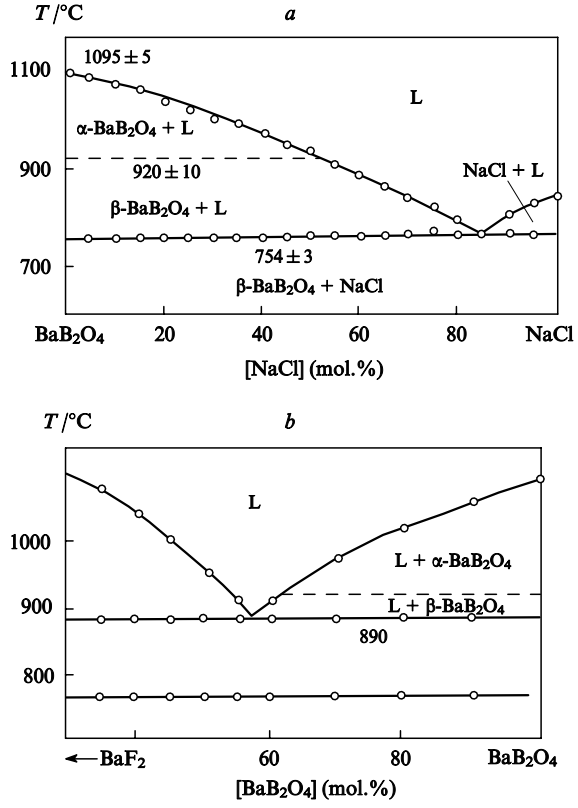


Figure 11. Phase equilibria in the systems BaB_2O_4–NaCl (see Ref. 124) (*a*) and BaB_2O_4–BaF_2 (see Ref. 122) (*b*).

NaF and $BaB_2O_4-BaF_2$ sections seem to be quasi-binary. The $BaB_2O_4-Na_2SO_4$ section is unstable, since in this case an exchange reaction occurs

$$BaB_2O_4 + Na_2SO_4 \longrightarrow BaSO_4 + Na_2B_2O_4 .$$

The temperatures of the eutectic in the BaB_2O_4-NaCl system, determined by different authors,[124,125] virtually coincide (see Fig. 11 *a*); however, the compositions of the eutectic are appreciably different. Correspondingly, the concentration ranges of the growth of β-BaB_2O_4 crystals in this system are also different. Data on the phase equilibria along the BaB_2O_4-NaF (see Refs 66 and 123) and $BaB_2O_4-BaF_2$ sections (see Refs 103 and 122) are contradictory.

All solvents studied have certain drawbacks. The systems containing Li_2O (see Ref. 103) and BaF_2 (see Ref. 122) exhibit very narrow crystallisation regions of β-BaB_2O_4, while no such region at all was found in the system containing CaF_2.[124] The system with $BaCl_2$ is characterised by fast hydrolysis. If fluoride melts are used, pyrohydrolysis also occurs in air,[128] either relatively fast (BaF_2) or slow (NaF). A number of additives (*e.g.*, MgF_2 and BaF_2) do not favour reduction of the melt viscosity; besides, the melt containing MgF_2 is prone to glass formation.[66] The use of lead-containing compounds [120,127] favours stabilisation of the α-modification of BaB_2O_4.[49] Potassium fluoride additives cause significant changes in the lattice parameters of BBO crystals, which seems to be due to isomorphous incorporation of potassium.[66]

The $BaO-B_2O_3-BaF_2$ system is used as flux in the growth of rare-earth ferrite single crystals.[129]

Sodium fluoride is considered as candidate for flux. The BaB_2O_4-NaF section and the $BaO-B_2O_3-NaF$ system are characterised by broad regions of primary crystallisation of β-BaB_2O_4 [66] and by substantial reduction of the viscosity of the melt, which permits crystallisation at higher rates. However, to make the best use of these advantages, the crystals should be grown in an inert gas atmosphere. Slow pyrohydrolysis of NaF in air during crystallisation causes a gradual transformation of the BaB_2O_4-NaF system into the $BaB_2O_4-Na_2O$ system.

Na_2O [45,46,64,86,90,91,101–103,105,121,124,130–146] is, at present, most widely used for melt-solution growth of β-BaB_2O_4 single crystals. Melt-solution growth of single crystals in the $BaB_2O_4-Na_2B_2O_4$ system has also been reported.[103] The process is complicated by high viscosity of the melt and its tendency to supercooling. A number of studies concerning variation of the melt composition in the $BaO-B_2O_3-Na_2O$ system are available.[64,134–137,143,144]

Phase equilibria in the $BaB_2O_4-Na_2O$ system were first studied by DTA[105] (cited according to Refs 46 and 130). A compound $Na_2BaB_2O_5$ was identified, which congruently melts at 846 °C. The temperatures of the eutectics are 755 and 573 °C. The phase diagram constructed by Huang and Liang [105] was used for the choice and 'tuning' of the growth regimes of BBO crystals.

Kaplun *et al.*[133] proposed yet another version of the phase diagram of the $BaB_2O_4-Na_2O$ system. In this case, the liquidus curve in the BBO crystallisation region and the eutectic position match those reported by Huang and Liang;[105] however, the compound $Na_2O \cdot BaB_2O_4$ was assumed to be incongruently melting at 830 ± 3 °C following a peritectic reaction resulting in a refractory compound that melts at temperatures above 1300 °C (this compound was assumed [133] to have a composition $3\,BaO \cdot B_2O_3$). An analogous interpretation of the phase equilibria in this system was reported in other studies.[143,144] The generalised phase diagram of the $BaB_2O_4-Na_2O$ system is shown in Fig. 12.

The region of primary crystallisation of β-BaB_2O_4 in the $BaO-B_2O_3-Na_2O$ ternary system (Fig. 13) has been thoroughly studied by Nikolov and Peshev.[64]

The contradiction between the results of studies[105,133] was solved recently.[102] In an investigation of the $BaB_2O_4-Na_2O$ section by DTA and visual-polythermal analysis (VPA) it was found (see Fig. 12) that both strong thermal effects (ascribed [105] to the melting of $Na_2BaB_2O_5$) and high-temperature equilibrium crystallisation (liquidus curve) manifest themselves in the concentration range from 30 mol.% to 50 mol.% Na_2O. These results are in agreement with those reported by Kaplun *et al.*[133] The medium-temperature effects were found [102] to be concentration dependent (this contradicts the results reported earlier [133]), which is impossible in the case of stable quasi-binary section.

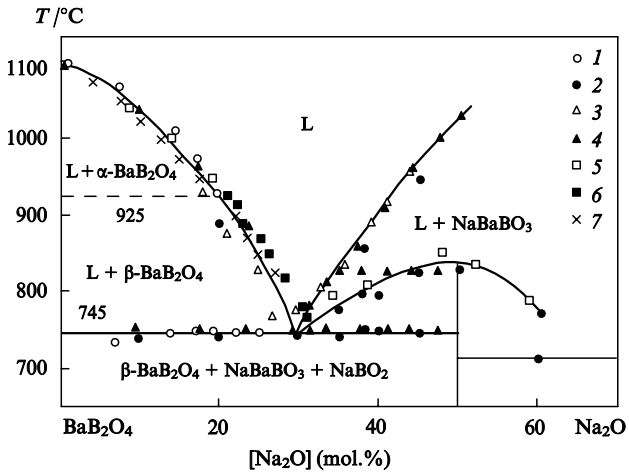


Figure 12. Phase equilibria along the $BaB_2O_4-Na_2O$ section.[102]
The data were obtained by DTA, the mixtures were prepared by successive addition of Na_2CO_3 to remelted BaB_2O_4 (*1*); the data were obtained by DTA, the samples were prepared by solid-phase synthesis (*2*); the data were obtained by visual-polythermal analysis (*3*); other data were taken from Ref. 133 (*4*), Ref. 105 (*5*), Ref. 64 (*6*) and Ref. 72 (*7*).

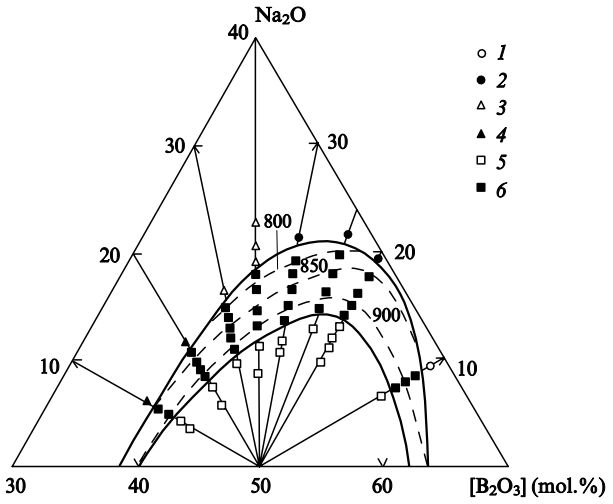


Figure 13. Primary crystallisation region of the α- and β-modifications of BaB_2O_4 in the $BaO-B_2O_3-Na_2O$ ternary system.[64]
Primarily crystallising phases: $Na_2B_4O_7$ (*1*), $NaBO_2$ (*2*), $Na_2BaB_2O_5$ (*3*), $Ba_3B_2O_6$ (*4*), α-BaB_2O_4 (*5*) and β-BaB_2O_4 (*6*). The dashed lines denote isotherms.

X-Ray diffraction and Raman spectroscopy studies showed that the reaction of BaB_2O_4 with Na_2O results in barium orthoborate, $NaBaBO_3$, whose structure comprises isolated $[BO_3]$ triangles and that compound $Na_2O \cdot BaB_2O_4$ does not exist. Single crystals of compound $NaBaBO_3$ were grown by spontaneous crystallisation from melts of different compositions including a melt containing 62 mol.% BaB_2O_4 and 38 mol.% Na_2O using a platinum loop seed. The compound melts at 1270 °C and undergoes a rapid degradation in air, being a good absorbent of water and carbon dioxide. The X-ray diffraction pattern of $NaBaBO_3$ is

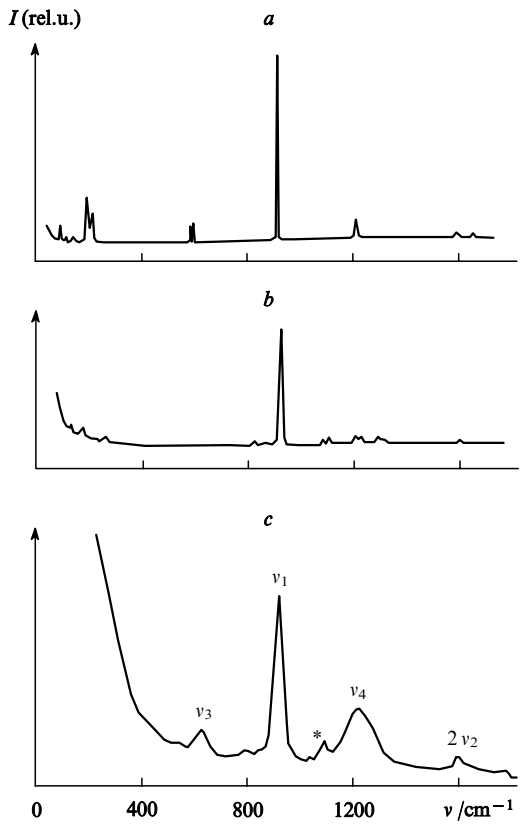


Figure 14. Raman spectra of a $NaBaBO_3$ single crystal (*a*), Na_3BO_3 powder (*b*) and 3 $Na_2O \cdot B_2O_3$ melt (*c*).[102]
The fundamental vibration of the impurity carbonate ion is asterisked.

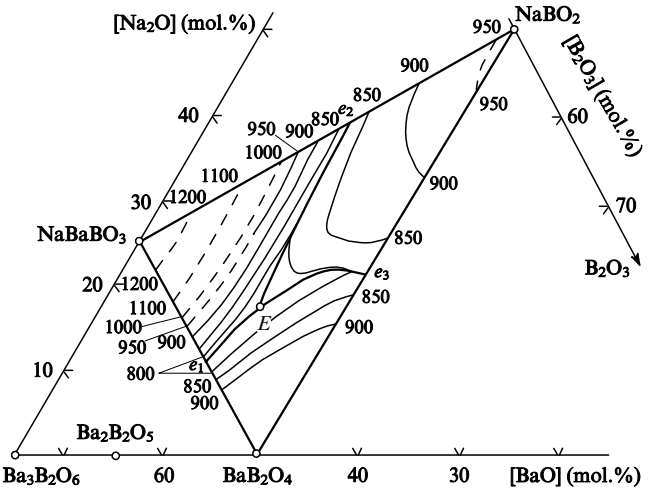


Figure 15. Projections of the liquidus surfaces in the BaB_2O_4–$NaBaBO_3$–$NaBO_2$ system on the concentration triangle.[102]
The eutectics are labelled e_1–e_3 and the ternary eutectic is labelled *E*.

shown in Fig. 8 *c* and its Raman spectrum is presented in Fig. 14 *a*.

Both the α- and β-modifications of BaB_2O_4 have nearly identical thermodynamic characteristics.[80, 82] This means that the liquidus curve (surface) corresponding to the polymorphic transformation of BaB_2O_4 should exhibit no kinks.

The projection of the liquidus surfaces of a part of the BaO–B_2O_3–Na_2O system on the concentration triangle is shown in Fig. 15. In this system, compound $NaBaBO_3$ is assumed to be congruently melting and the BaB_2O_4–$NaBO_2$, $NaBaBO_3$–$NaBO_2$ and, probably, BaB_2O_4–$NaBaBO_3$ sections are thought to be of eutectic character (the eutectics lie at 28 mol.% BaO, 50 mol.% B_2O_3, 22 mol.% Na_2O, 826 °C and at 22 mol.% BaO, 39 mol.% B_2O_3, 39 mol.% Na_2O, 830 °C). The region of primary crystallisation of $NaBaBO_3$ can be determined by analysing the morphology of the primary (spontaneously grown) crystals. The primary crystals are isometric individuals in contrast to needle-shaped BaB_2O_4 and $NaBO_2$ crystals. The ternary eutectic occurs at 745 °C and lies at 41 mol.% BaO, 41 mol.% B_2O_3, 18 mol.% Na_2O (or 70 mol.% BaB_2O_4, 30 mol.% Na_2O). The results obtained by different authors [64, 102] are in good agreement.

By chance, the BaB_2O_4–Na_2O section passes nearly exactly through the ternary eutectic in the BaB_2O_4–$NaBaBO_3$–$NaBO_2$ ternary system. Therefore, the left part of the BaB_2O_4–Na_2O section looks like a binary system. It seems likely that weak high-temperature effects were overlooked [105] and that the non-variant effect of the L + $NaBaBO_3$ + $NaBO_2$ binary eutectic was interpreted to be the melting of a compound $BaB_2O_4 \cdot Na_2O$, while the co-crystallisation (co-melting) curve of $NaBaBO_3$ + $NaBO_2$ was considered to be the liquidus curve.

Studies of the phase diagram of the BaO–B_2O_3–Na_2O system are complicated by high reactivity and hygroscopicity of melts, by their ability to absorb carbon dioxide and by the corroding action of the melts on the platinum crucibles. High viscosity of the melts and their tendency to supercooling, glass formation and appearance of metastable equilibria present a particular problem.[102, 143–145]

According to the phase diagram of the BaB_2O_4–Na_2O section (see Fig. 12), the temperature range of crystallisation of β-BaB_2O_4 is ~170 °C. The compositions suitable for growth of the low-temperature phase lie in the range 22 mol.%–30 mol.% Na_2O. Usually, the composition with the Na_2O content between 20 mol.% and 22 mol.% is used as charge. However, supercooling of the melt allows growth of large β-BaB_2O_4 crystals at a Na_2O content of less than 5 mol.% at ~1050 °C.[121]

The volatility of the melt increases along the BaB_2O_4–Na_2O section, whereas its viscosity decreases as the concentration of Na_2O increases.[121, 132, 145]

b. Crystal growth techniques

The driving force of the melt-solution growth of BBO crystals is due to temperature reduction. Usually, vaporisation of the solvent is not used as a method for the preparation of a supersaturated solution.[117–119] The process can be performed using various equipment.

Schematical illustrations of a number of crystal growth techniques are shown in Fig. 10.

Only a few studies are concerned with the growth of (i) BBO single crystals by the travelling solvent method (a version of zone melting technique),[131] (ii) single-crystal filaments by laser-assisted pulling from pedestal [120] and (iii) plates using the Stepanov technique.[85, 92]

The so-called top-seeded solution growth (TSSG) technique is most widely used.[45, 46, 66, 86, 121, 130, 137–140, 146] It allows bulk BBO crystals (up to 60 mm in diameter and more than 10–15 mm long) to be grown (Fig. 16). Several versions of this method are known. If crystal growth occurs on slow cooling of the melt without pulling the seed, one deals with the Kyropoulos technique. The Czochralski method involves pulling of the seed-growing crystal under isothermal conditions (see Fig. 10).

In the case of melt-solution crystallisation the composition of the crystal differs from that of the melt; therefore, a feature of the Czochralski technique is continuous change in the composition of the melt and, correspondingly, in the crystallisation conditions. To avoid variations of the melt composition and other parameters and to maintain steady-state growth conditions, a method involving melt feed with BBO charge was proposed.[132]

Often, a combination of the two above-mentioned growth techniques is employed. In this case, a slow pulling of the crystal is

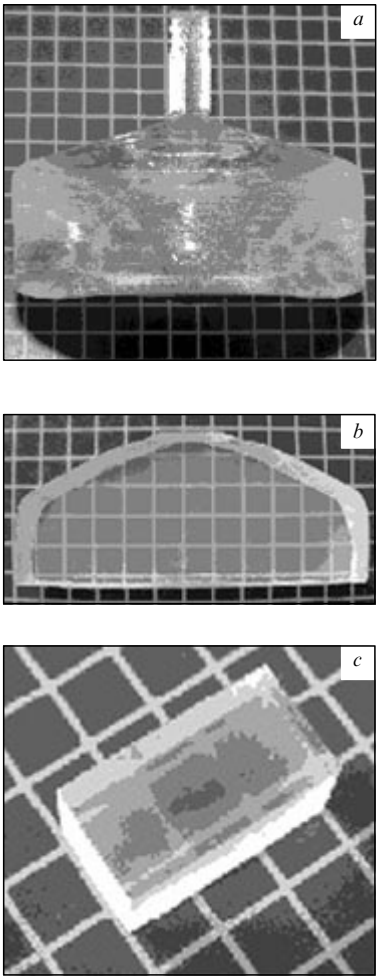


Figure 16. Photographs of a BBO crystal (*a*), axial slice 8 mm thick (*b*) and a nonlinear optical element of dimensions $8 \times 8 \times 15$ mm^3 (*c*). Paper cell size is 5×5 mm. The crystal was grown by the authors of this review at the Crystal Growth Laboratory, Institute of Mineralogy and Petroghaphy, Siberian Branch of the Russian Academy of Sciences.

combined with slow cooling of the melt. The major advantages of the TSSG technique with pulling of the crystal compared to analogous technique without pulling are as follows:

— higher crystal growth rate;

— the possibility of growing thick crystals in smaller crucibles;

— prevention the crucible walls from touching with the growing crystal, which causes seed failure.

Seed growth of bulk β-BaB_2O_4 crystals of good quality with and without pulling from Na_2O flux has been reported.[121] The seed rotation rate varied from 2 to 60 rpm while the pulling speed was 0.01 – 0.02 mm h^{-1}. The high seed rotation and crystal pulling rates cause undesired changes in the shape of the interface from a convex interface to a concave one. Inclusion-free BBO crystals were grown at low pulling rates (of the order of 0.5 to 1.0 mm per day).

As a rule, a melt of composition 75 mol.% BBO – 25 mol.% Na_2O was used. The liquidus temperature for this composition is ~886 °C. The starting reagents ($BaCO_3$, H_3BO_3 and Na_2CO_3) were weighed, mixed and placed in a platinum crucible 75 mm in diameter. Then the crucible was heated to ~1110 °C over a period of several hours until complete decomposition of carbonates. Seed crystals with different orientations were used for crystal growth. Orientation of the seed crystal affects not only the rate and quality of growth, but also the shape of the BBO crystal. A high anisotropy of the growth rate of BBO crystals was reported. The rates of growth along the *a* and *b* axes were found to be higher than the rate of growth parallel to the *c* optical axis. Crystals grown parallel to the *a* and *b* axes or in other directions that strongly deviate from the *c* axis usually undergo spontaneous cracking in the (001) cleavage plane. This is due to anisotropy of the thermal expansion. The thermal expansion and thermal conductivity coefficient of BBO crystals measured along the *c* axis are by nearly an order of magnitude larger than those measured in the perpendicular direction.[39]

The radial and axial temperature gradients and the shape of the liquid – solid interface are important parameters that define quality of the crystal. Crystals of the best quality are usually grown if the interface is flat or slightly convex. The shape of the interface depends on both the pulling speed and the seed rotation rate. Obtaining a flat or slightly concave interface requires that the pulling speed and the seed rotation rate be 0.5 – 1.0 mm per day and 4 – 8 rpm, respectively. As the seed rotation rate increases, the contribution of forced convection gradually becomes much larger than that of natural convection. If the pulling speed seed is too high, the growing crystals can lose contact with the solution.

Search for methods of control of convective heat and mass transfer always has received considerable attention, since it is these processes that in most cases provide the possibility of growing particular types of crystals with preset properties. All methods of control can be divided into contact methods and contactless ones. The former are based on the action of a physical body placed in contact with the melt, solution or another crystallisation medium. Most of these methods involve mechanical rotation of the crystal and/or crucible, the use of various diaphragms, stirrers, shape-forming elements, *etc*. A number of contact methods have been applied to the growth of BBO crystals.[139, 147, 148] Extreme sophistication of the mechanical devices gave an impetus to search for simpler methods of control of the heat and mass transfer processes. This approach had some success.

Contactless techniques are based on the action of physical fields (gravitational, electromagnetic and thermal) on the heat and mass transfer processes.

In practice, all crystal growth techniques include (sometimes, unconsciously) a certain pattern of the heat field. In most cases these are static heat fields characterised by the symmetry axis of an infinite order, L_∞, and particular values of the axial and radial temperature gradients. Traditionally, crystals are grown in tube heating furnaces with cylindrical heat field symmetry L_∞ (excluding the edge effects). With the advent of precision heating furnaces (PHF),[149] the possibility of controlling the heat field and the heat and mass transfer during the crystal growth appeared. This is achieved by changing the heat field symmetry and by rotating the heat field. A version of dynamic control of the heating elements (HE) in such a furnace has been reported.[150 – 153] In practice, the growth of crystals under conditions of static, azimuthally distributed heat field in the PHF is also of considerable interest.[140] These conditions are created by either commutation or regular arrangement of the HE around the PHF muffle, which provides a radially distributed pattern for power delivered to the muffle walls and, hence, to the walls of the growth crucible.

Experiments on the growth of BBO crystals [140] were carried out using a heating furnace with a total of 18 HE arranged evenly around the quartz muffle 110 mm in diameter with walls 4 mm thick. Switching on all series-connected HE in the furnace produced a heat field of cylindrical symmetry L_∞. Strictly speaking, in this case the heat field symmetry should be L_{18}; however, it was considered as L_∞ (within the limits of experimental error) due to the choice of an optimum distance between the HE and taking into account the effect of the heat field smoothing by the muffle and the crucible walls. Switching off each third HE changed the heat field symmetry in the furnace to six-fold symmetry L_6. If three HE arranged at an angle of 120 ° with respect to one another were switched off, the heat field symmetry reduced to L_3. In

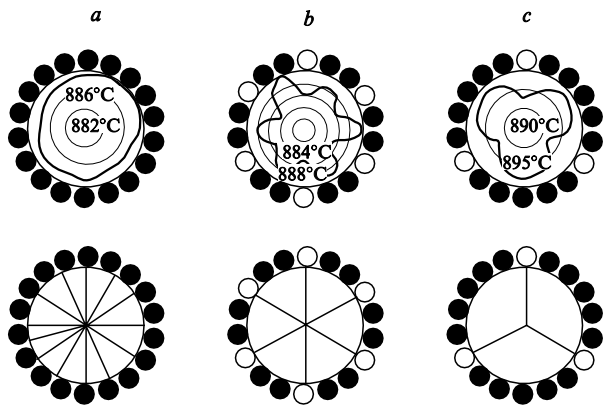


Figure 17. Polar diagrams of the heat fields of symmetry L_∞ (*a*), L_6 (*b*) and L_3 (*c*) used for the growth of BBO crystals (at the top) and the corresponding convective patterns (at the bottom). The open circles denote the switched off heating elements.

Fig. 17, we present the horizontal sections of the growth furnace and the polar diagrams of the heat fields of symmetry L_∞, L_6 and L_3, as well as the typical convective patterns on the melt-solution surface, formed under the action of the heat fields of different symmetry.

BBO crystals were grown on a 4×4 mm seed oriented parallel to the optical axis *c*. The growth procedure consisted in search for an equilibrium temperature by seed touching the melt-solution surface in the place where the rays of the convective star are brought to a point. After the seed started to spontaneously dissolve, the temperature in the furnace was lowered by 1–2 degrees. The next touching of the melt surface was performed after 2–3 h. After prolonged (12–24 h) liquid–seed contact the crystal was allowed to grow on cooling the furnace at a rate of 1–3 degrees per day. The seed was rotated at 1–2 rpm and moved upward at a rate of 0.3–0.4 mm per day. The growth process continued until the crystal became visually much less transparent. This was interpreted as an indication of the constitutional supercooling, which induced a cellular crystal growth.

The experimental data on the growth of BBO crystals under the action of steady-state heat fields of different symmetry are listed in Table 3. As can be seen, a change in the heat field symmetry from L_∞ to L_6 led to a slight increase in the 'yield' coefficient (from 1.22 ± 0.02 to 1.27). However, the 'yield' coefficient increased by a factor of 1.7 to 2.07 g (kg deg)$^{-1}$ on going to L_3 symmetry [*cf.* a theoretical value of $\sim$2.52 g (kg deg)$^{-1}$ obtained according to the liquidus equilibria in the BaB_2O_4–Na_2O system].

Table 3. Experimental data on BBO crystals grown in a crucible 100 mm in diameter at initial charge of 1.5 kg in heat fields of different symmetry.[140]

Run No.	Heat field symmetry	ΔT/°C	Pulling /mm	Crystal mass /g	'Yield' coefficient [a] /g (kg deg)$^{-1}$
1	L_∞	117.5	12.6	212	1.20
2	L_∞	122.9	10.3	227	1.23
3	L_∞	106.4	16.7	198	1.24
4	L_6	94.2	14.2	179	1.27
5	L_3	103.0	14.4	319	2.07

[a] The 'yield' (or 'mass production') coefficient is an increase in the mass of a crystal grown upon 1 °C temperature reduction at initial crucible charge of 1 kg.

The changes in the 'yield' coefficient as function of the heat field symmetry and the observed character and evolution of convective flows on the melt surface were interpreted as follows.[140] As the heat field with L_3 symmetry was created in the growth furnace, the convective regime in the bulk of the melt changed fundamentally. The fluid body divided into three azimuthally distributed convective cells in which the thermal-gravitational flows moved up and down, thus 'enveloping' nearly the whole bulk of the liquid phase and forming three intense surface flows merging at the centre. This convective regime provided a permanent renewal of the melt in the region near the crystallisation interface, thus substantially delaying the onset of constitutional supercooling. In this case the 'yield' coefficient amounted to 82% of its maximum theoretical value. This, in a way, characterises the extent of involvement of the fluid body in the convection.

BBO crystals thus obtained were found to have a very small central defect region. These crystals can be used for fabrication of relatively large (up to 20 mm and more) nonlinear optical elements and electro-optical cells oriented parallel to the optical axis *c* .

Feigelson *et al.*[130] reported the 'yield' coefficients of 2.01 and 2.13 g (kg deg)$^{-1}$ obtained in the growth of BBO crystals from a crucible 55 mm in diameter with the corresponding initial charges of 380 and 290 g. An increase in the charge to 470 g caused reduction of the 'yield' coefficient to 1.6 g (kg deg)$^{-1}$. This points to significant difference between the convective regimes in the crucibles 55 and 100 mm in diameter at comparable temperature gradients in the growth furnace.

Recently,[154] pioneering results concerning the growth of BBO crystals in rotating heat fields of different symmetry have been reported.

VIII. Defects and impurities in crystals

Information on intrinsic nonstoichiometry and impurity defects in BBO crystals is scarce.[155] Three types of radiation defects that exhibit UV absorption at 210, 250 and 310 nm were identified in γ-irradiated BBO crystals. The formation of these defects is assumed to be associated with both cleavage of the B–O bonds and atomic displacements from the equilibrium positions.[156]

Growth defects were studied by chemical etching, optical microscopy, microprobe technique, X-ray topography and laser scanning tomography.[46, 86, 121, 130, 157, 158] The main types of defects found in BBO crystals were inclusions (usually, they are interpreted as flux inclusions) and inclusion-induced dislocations. The appearance of gas bubbles is associated with the presence of trace amounts of non-decomposed carbonates in the charge.[86] High density of dislocations due to solvent trapping was pointed out.[121] It is assumed that removal of inclusions must favour a substantial improvement of the quality and optical characteristics of BBO crystals.

The content of sodium in β-BaB_2O_4 crystals grown under different conditions (from melt-solution and from a stoichiometric melt according to Czochralski) can vary from 120 to 680 ppm (0.012 mass %–0.068 mass %).[159] Transparent inclusion-free crystals contain from 0.012 mass % to 0.023 mass % Na. At a sodium content of greater than 0.035 mass %, the crystals are semi-transparent until becoming opal. Sodium impurity was found to be responsible for thermoluminescence of BBO crystals.[159, 160]

Among other impurities, an increased concentration of strontium was pointed out.[161] Probably, this impurity incorporates into the BBO crystals from barium-containing starting reagents. Lead impurity causes stabilisation of the α-modification of BaB_2O_4.[49]

A feature of BBO crystals is accumulation of sodium and potassium impurities.[101] The critical concentration of sodium is 0.021 mass %. As the content of sodium exceeded this value, inclusions of the second phase and the scattering centers appear.[101] The effective distribution coefficient of sodium between the crystal and melt is $(2.5–4.4) \times 10^{-3}$.

From crystal chemical considerations it follows that alkali metal impurities can incorporate into the structure of β-BaB_2O_4. As can be seen in Fig. 7, BaB_2O_4 and a sodium compound $NaBO_2$ are structurally similar. They contain identical structural fragments (boron – oxygen $[B_3O_6]^{3-}$ anions) stacked perpendicular to the *c* axis of the trigonal lattice and exhibit a similar packing motif. The difference is in the arrangement of cations; the number of sodium ions that provide electrostatic compensation of charge is twice as large as the number of barium ions. The trigonal unit cells also have close parameters (see Table 1). This suggests the possibility of heterovalent isomorphism simply described as $Ba \rightleftarrows 2\,Na$ and incorporation of extra sodium ions into the β-BaB_2O_4 lattice. The authors of this review also assume that the major type of intrinsic point defects in β-BaB_2O_4 crystals are Frenkel pairs characterised by displacement of Ba ions from the equilibrium positions to the interstitial ones. Close values of the unit cell parameters allow epitaxial growth of $NaBO_2$ on the β-BaB_2O_4 crystals.

Even better is agreement between the lattice parameters of β-BaB_2O_4 and potassium metaborate, KBO_2, which is isostructural to the sodium-containing analogue. Potassium ions are readily incorporated into the BBO lattice (potassium fluoride melt was used as flux).[66]

The distribution coefficient of sodium in BBO crystals is small, therefore this impurity can be removed by zone melting with ease.[88] Low efficiency of this technique in the removal of strontium impurity from BBO crystals[107] indicates that the corresponding distribution coefficient approaches a unity.

Inclusions in BBO crystals were found to be sodium enriched.[46, 130] Identification of the phase that is formed at the crystallisation interface, thus blocking the process of crystal growth, by X-ray powder diffraction failed.[66] However, a recent X-ray powder diffraction study of the particles with inclusions, picked up with a microscope, showed[102] that this phase has a composition $NaBaBO_3$.

IX. Constitutional supercooling

Morphological instability of the crystallisation front (Fig. 18) occurs in a certain stage of melt-solution growth of BBO crystals (usually, as the crystal becomes ~15 mm thick). It involves the development of a characteristic cellular substructure with quasi-hexagonal cells, which is accompanied by trapping of inclusions and the formation of a protrusion.[46, 66, 130] The appearance of cellular substructure is the major reason for forced termination of the process of crystal growth. This phenomenon is associated with specific features of heat transfer during the growth process.[130, 143] However, usually the morphological instability is due to the constitutional supercooling which has been studied in detail for binary systems.[162–166]

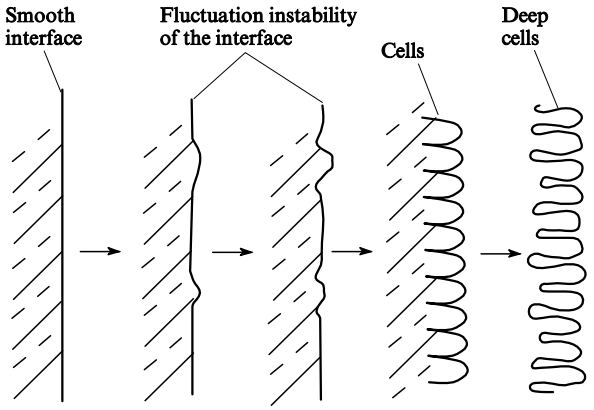


Figure 18. Qualitative picture of the development of morphological instability of the crystallisation front and the formation of cellular substructure.

Consider the growth of BBO crystals from a Na_2O melt-solution. In this case, sodium piles up near the solidification front, thus causing the loss of its stability. Figure 19 presents a scheme illustrating the distribution of the melt components in the region adjacent to the solidification front for a steady-state growth of BBO crystals from Na_2O melt-solution at the rate *R*. Since the amount of sodium incorporated into the crystal is very small, it is displaced by the growing crystal and is accumulated near the liquid – solid interface. The sodium concentration jump appeared at the crystallisation front induces a diffusion flow of sodium ions in the melt, which is directed away from the liquid – solid interface. The content of barium and boron in the melt is somewhat lower than in the crystal; therefore, these components are trapped by the crystal. This leads to the appearance of a region depleted of Ba and

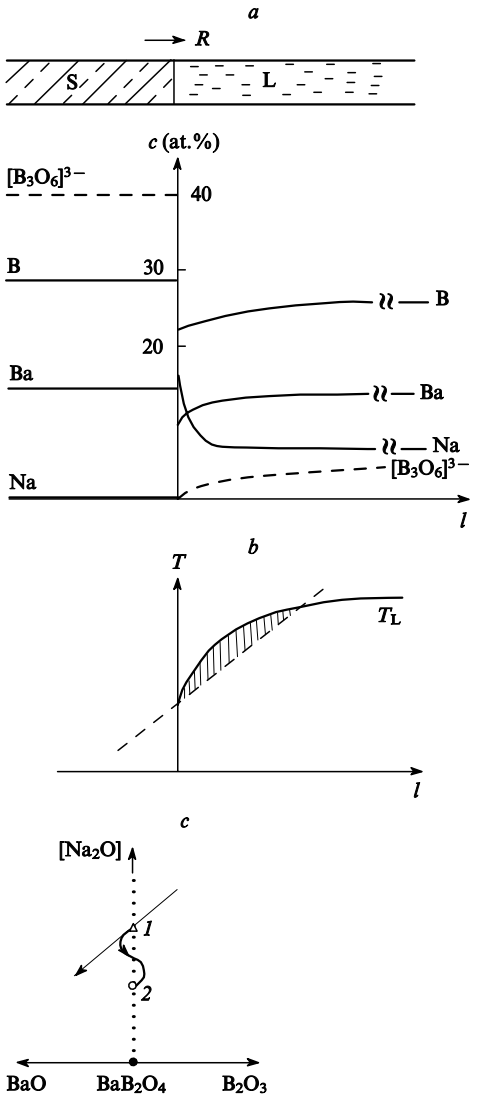


Figure 19. Schemes illustrating the distributions of the B, Ba, Na and $[B_3O_6]^{3-}$ ring ion concentrations in the crystal – melt system for a steady-state directional crystallisation occurring at a rate *R* (*a*), of the equilibrium crystallisation temperature of β-BaB_2O_4 (solid line) and of actual change in the temperature (dashed line) (*b*), and the hypothetical change in the melt composition with the distance from the solidification front (diffusion path) during the growth of BBO crystals (*c*).[104]
Shown are the constitutional supercooling region (*b*, hatched), the melt composition at the solidification front (*c*, *1*) and the starting composition of the melt (*c*, *2*).

B near the crystallisation front and induces diffusion flows directed from the bulk of the melt towards the interface. Accumulation of the excess sodium should reduce the equilibrium liquidus temperature. The integrated distribution curve of the equilibrium crystallisation temperature is presented in Fig. 19 *b* while the possible shift of the figurative point corresponding to the melt composition for actual crystallisation is shown in Fig. 19 *c*. Since the $BaB_2O_4 - Na_2O$ section is unstable, the line corresponding to the change in the melt concentration with distance from the solidification front (diffusion path) should deviate from this section, thus forming a zig-zag curve on the concentration triangle.[167]

More detailed analysis of the situation requires a consideration of different forms of boron present in the melt. As mentioned above, melting of BaB_2O_4 causes destruction of the $[B_3O_6]^{3-}$ ring anions (*i.e.*, this crystal is a typical example of compound which nearly completely dissociates on melting).[99, 100, 112] According to the molecular dynamics calculations,[168] the addition of Na_2O to the melt leads to shortening of the $[BO_2]_n^{n-}$ polymer chains formed by $[BO_3]^{3-}$ triangles and to an increase in the proportion of isolated $[BO_3]^{3-}$ triangles, dimeric $[B_2O_5]^{4-}$ units, three-membered $[B_3O_7]^{5-}$ fragments and $[B_3O_6]^{3-}$ ring anions. Nevertheless, one can state that it is the low concentration of the $[B_3O_6]^{3-}$ ring anions near the crystallisation front that is the limiting factor for the growth of BBO crystals.

It should be noted that steady-state melt-solution growth of BBO crystals can be performed using the Czochralski method with melt feed [132] or by floating zone technique.[131] Experiments carried out according to Kyropoulos (with slow cooling of the system) represent a kind of non-steady-state processes characterised by accumulation of sodium near the solidification front (Fig. 20).

The simplest constitutional supercooling criterion for solidification front stability is provided by the Tiller – Chalmers criterion

$$\frac{GD}{R} < \frac{mC_0(1-k)}{k},$$

where G is the temperature gradient in the melt at the solidification front, D is the diffusion coefficient of the solute, R is the crystal growth rate, m is the slope of the liquidus curve, C_0 is the concentration of the solute in the solution and k is the partition coefficient. This criterion was proposed for steady-state processes in dilute binary systems [162, 163] and cannot be applied to the crystallisation of BBO. This criterion is equivalent to the boundary condition at the crystallisation interface while the integrated curve describing the increase in the equilibrium crystallisation temperature (liquidus temperature) with the distance from the solidification front of BBO follows the same pattern as in the case of binary systems. Therefore, the criterion for morphological stability of the solidification front of BBO (heat transfer is assumed negligible) can be written as follows

$$\frac{G}{R}D^* < \mathbf{m}\Delta\mathbf{C},$$

where D^* is the function of the diffusion coefficients of the components of the system in the melt (it varies from one composition to another), **m** is the directional derivative of the liquidus temperature taken along the tangent to the diffusion path at the point corresponding to the melt composition at the solidification front (this point is labelled *1* in Fig. 19 *c*) and **ΔC** is the change in the composition at the interface. An analogous expression proposed[166] for binary systems can also be used for non-steady-state processes.

In any case the most important factors improving the stability of the solidification front against constitutional supercooling are an increase in the temperature gradient at the crystallisation front and a decrease in the crystal growth rate.

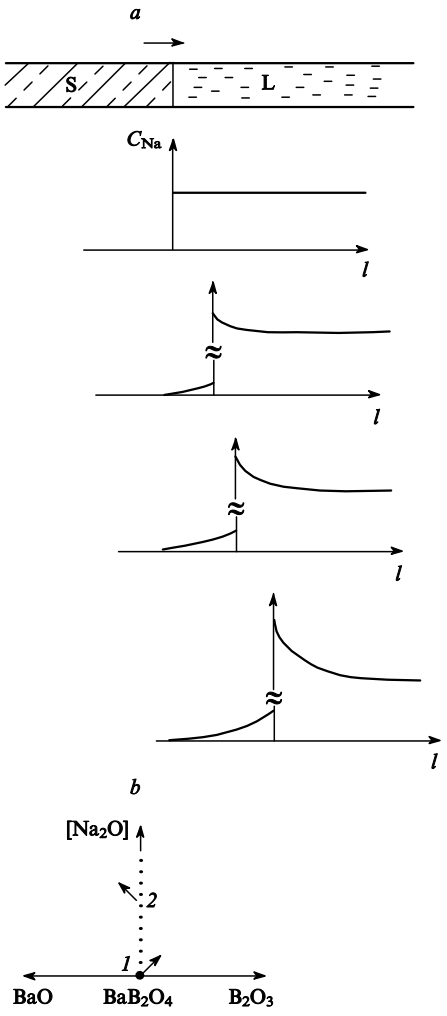


Figure 20. Schemes illustrating successive accumulation of sodium ahead of the crystallisation front for a non-steady-state growth of BBO crystal (*a*) and the change in the sodium content in the crystal (*1*) and in the melt (*2*) (*b*).

There are two reasons for deterioration of the optical quality of flux grown BBO crystals. These are (i) the attainment of critical supersaturation with respect to sodium near the crystallisation front and (as a consequence) the appearance of a cellular structure with trapped inclusions and (ii) accumulation of sodium impurity above the equilibrium solubility (limiting concentration) in BBO followed by crystallisation of the second phase on cooling of the crystal. In both cases mixing of the melt for not only control of the heat convection, but also homogenisation of the melt composition is of paramount importance.

X. Properties and fields of application of β-BaB_2O_4 crystals

Crystals of the non-centrosymmetric low-temperature modification, β-BaB_2O_4, are widely used in nonlinear optics as nonlinear-optical crystals possessing large birefringence for the generation of optical harmonics and sum frequencies of laser radiation in the visible and UV regions. Widespread use of this material in quantum electronics is to a great extent due to relatively high optical damage threshold. Numerous applied [30, 169 – 195] and materials science studies [156, 157, 196 – 201] of BBO were reported in the last decade.

Development of compact solid-state sources of tunable UV, visible and IR radiation is topical. Currently, BBO-crystal para-

metric light oscillators (OPOs) pumped by the second and third harmonics of Nd : YAG lasers are most widely used. These devices generate tunable radiation in the 2628 and 3036 nm regions, respectively.[192] The tuning range of BBO-crystal OPOs is limited to strong absorption of the idler wave radiation in the spectral region from 2200 to 3000 nm.[44] The pioneering study of the characteristics of a BBO-crystal OPO pumped by the fourth harmonic of a Nd : YAG laser ($\lambda = 266$ nm) was reported by Bosenberg *et al.*[193] A BBO-crystal OPO 25 mm long generated radiation in the spectral region between 330 and 1370 nm at a pulsed pump intensity exceeding 23 MW cm^{-2}. Another BBO-crystal OPO pumped by the fourth harmonic of a single-mode Nd : YAG laser generated radiation in the region 302 – 2248 nm at a pulsed pump energy of 20 mJ with a conversion efficiency of 6.3% at a wavelength of 340.2 nm at quadruple the oscillation threshold.[192]

The characteristics of a BBO-crystal Type-I OPO pumped by the fourth harmonic of a multimode Nd : YAG laser have been studied.[194] The output was tunable over the region 300 – 2340 nm. The efficiency ranged up to 15% near the peak of the tunability curve at double the oscillation threshold. The OPO configuration was based on a BBO crystal (aperture 6×8 mm, length 14 mm) cut for Type-I phase matching at an angle (θ) of 38.3 ° with respect to the optical axis of the crystal.

The above-mentioned applications of BBO crystals were based on the second-order optical nonlinearity. However, β-BaB_2O_4 also possesses third-order optical nonlinearity.[30] In particular, it was found that picosecond laser pump of BBO at 1 μm excites efficient Stokes and anti-Stokes Raman parametric generation (RPG) and allows simultaneous SHG and multicomponent RPG in the visible and near IR regions. In particular, a BBO-crystal active element 15 mm long [excitation configuration *a*(*cc*)*a*] pumped at 1 μm re-emitted to all RPG components more than 35% of the energy (~1 mJ), the first Stokes line ($\lambda = 1.1414$ μm) accounting for ~20%. The efficiency of picosecond RPG from β-BaB_2O_4 was also illustrated by an extended (up to the thirteenth component with $\lambda = 0.5661$ μm) wing of the multicomponent anti-Stokes spectral region. Based on high SHG efficiency of BBO crystals, an SRS experiment with the optically active element oriented parallel to the Type-I phasematching direction (*ee-o*) was carried out.[30] The experiments showed the possibility of simultaneous conversion of the 1 μm pump of BBO into both the Stokes and anti-Stokes components and the second harmonic. It was found that excitation of the multicomponent RPG induced by the second harmonic generated by the BBO crystal occurs at a lower pump power, which is due to high SHG efficiency from BBO crystals and to dispersion of the Raman amplification coefficient of BBO. This discovery — simultaneous manifestation of the second- and third-order optical nonlinearities in BBO crystals — can be used for creation of novel types of β-BaB_2O_4-based laser frequency converters.

Electro-optical application of BBO crystals as Pockels cells in the UV spectral region should be emphasised.[195]

Recently, BBO crystals have been on the commercial market. A large body of valuable information on the physicochemical properties of BBO crystals can be found in the Internet at URLs http://www.crystaux.com/betabbo.htm (website of DLK Crystal) and http://www.clevelandcrystals.com/BBOLBO.shtml (website of Cleveland Crystals, Inc.). The principal properties of BBO crystals are listed in Table 4.

Table 4. Properties of BBO single crystals.

Parameter	Value
Optical transmission /nm (50% transmission at a thickness of 3 mm)	0.196 – 2.2
Indices of refraction [a] at λ	
0.2660 nm	1.7571; 1.6146
0.4358 nm	1.6868; 1.55638
0.5461 nm	1.6738; 1.5547
0.6328 nm	1.6673; 1.5500
1.0642 nm	1.6551; 1.5425
Absorption coefficients α (cm^{-1}) at λ	
0.266 nm	0.04 – 0.15
1.0 nm	0.001 – 0.002
2.09 nm	0.0085; [b] 0.07 [c]
Laser damage threshold /GW cm^{-2} at $\lambda = 1.0642$ nm	
10 ns pulse	0.0046
0.1 ns pulse (2.3 J)	15
Nonlinear optical susceptibility /pm V^{-1}	2.3; [d] < 0.1 [e]
Phasematching range (λ /nm)	
Type I SHG	0.4096 – 3 +
Type II SHG	0.53 – 3 +
Phasematching angle [f] (deg) at maximum nonlinear optical susceptibility and 25 °C	
0.532 nm, type I SHG	47.6; 90
0.532 nm, type II SHG	81.0; 0
1.064 nm, type I SHG	22.8; 90
1.064 nm, type II SHG	32.8; 0
Linear electro-optical coefficients [g] /pm V^{-1}	2.7 ± 0.4; ~0; 0.055
Hardness, Mohs	4.5
Elastic stiffnesses /GPa	
c_{11}	123.8
c_{12}	60.3
c_{13}	49.4
c_{14}	12.3
c_{33}	53.3
c_{44}	7.8
c_{66}	31.8
Young's modulus /GPa	39
Poisson's ratio	0.58
Thermal expansion coefficient, [i] 10^{-6} (deg)$^{-1}$	4; 36
Specific heat /J (g deg)$^{-1}$	0.49 ± 0.02
Thermal conductivity /W (m deg)$^{-1}$	
parallel to *c* axis	1.6
perpendicular to *c* axis	1.2
Resistivity /Ω cm	$> 10^{11}$
Relative static dielectric constants [k]	6.7; 8.1

[a] The n_0 and n_e values are respectively given. [b] *e*-Ray. [c] *o*-Ray. [d] The d_{22} value. [e] The d_{15} value. [f] Given are the θ and Φ values, respectively. [g] Listed are the r_{22}, r_{31} and r_6 values, respectively. [i] Given are the α_a and α_c values, respectively. [k] Given are the $\varepsilon_{11}/\varepsilon_0$ and $\varepsilon_{33}/\varepsilon_0$ values, respectively.

XI. Conclusion

Based on the aforesaid, the following conclusions can be drawn.

Polymorphism of BaB_2O_4 is a unique phenomenon. On the one hand, the high- and low-temperature modifications of this compound have substantially different structures. On the other hand, their thermodynamic characteristics are nearly identical. Studies of the mutual stability of these modifications and of the influence of different factors on their crystallisation and kinetics of transformations are of great importance. In this connection, investigations of the heat capacities of both modifications of BaB_2O_4 over a wide temperature range are also required.

Hübner's data [62, 65] on the stability of compound $Ba_2B_2O_5$ and on the formation of BaB_2O_4-based solid solutions strongly contradict the phase diagram of the $BaO - B_2O_3$ system proposed by Levin *et al.*[12, 13] An indirect proof of variable composition of BBO is provided by small but, at the same time, noticeable variations of the lattice parameters of single crystals, determined by different authors. Both nonstoichiometry of BaB_2O_4 and the $BaO - B_2O_3 - Na_2O$ system in the BaO-enriched region (in particular, in the $Ba_3B_2O_6 - NaBaBO_3 - BaB_2O_4$ concentration triangle) call for further investigation.

Studies of the phase equilibria in the $BaO-B_2O_3-Na_2O$ ternary system showed that the $BaB_2O_4-Na_2O$ section, which is most often used for growth of β-BaB_2O_4 single crystals from Na_2O, is unstable and that compound $Na_2BaB_2O_5$ does not exist. Compound $NaBaBO_3$ was identified and structurally characterised. The $BaB_2O_4-Na_2O$ section passes nearly exactly through the eutectic in the $BaB_2O_4-NaBaBO_3-NaBO_2$ ternary system.

The $BaB_2O_4-Na_2O$ melt used for growth of BaB_2O_4 crystals is multicomponent and unstable. Further search for optimum growth conditions and better solvents seems to be appropriate.

Improvement of methods of control of the heat and mass transfer during crystal growth including those involving variation of the heat field patterns is also topical.

This review has been performed as part of the Research Project 'Investigations of the Phase Diagrams, Search for Solvents and Growth of Nonlinear Optical Crystals in Heat Fields of Different Symmetry' carried out in the framework of the Integration Programme 'Novel Principles and Methods of Design and Targeted Synthesis of Chemical Compounds with Preset Properties' in accord with the Decision of the Presidium of the Siberian Branch of the Russian Academy of Sciences signed on 09.04.2002.

The authors express their gratitude to P Peshev (Institute of General and Inorganic Chemistry, Bulgarian Academy of Sciences, Sophia) for providing access to valuable information, to R M Zakalyukin, E A Tkachenko (A V Shubnikov Institute of Crystallography, Russian Academy of Sciences, Moscow) and S V Kuznetsov (M V Lomonosov Moscow State Academy of Fine Chemical Technology) for technical support and to Yu V Pisarevskij (A V Shubnikov Institute of Crystallography, Russian Academy of Sciences) and A M Yurkin (Institute of Mineralogy and Petrography, Siberian Branch of the Russian Academy of Sciences) for valuable help.

References

1. R Benedikt *Ber. Detsch. Chem. Ges.* **7** 703 (1874)
2. *Gmelin Handbuch der Anorganichen Chemie* (Berlin: Verlag Chemie, 1932)
3. *Gmelin Handbuch der Anorganichen Chemie. Borverbindungen. Boroxide. Borsauren. Borate* (Berlin; Heidelberg; New York: Springer, 1975) Bd 28, Teil 7
4. A D Keshan *Sintez Boratov v Vodnom Rastvore i ikh Issledovanie* (The Synthesis of Borates in Aqueous Solution and Investigation of Them) (Riga: Izd. Akad. Nauk Latv. SSR, 1955)
5. G K Gode, Doctoral Thesis in Chemical Sciences, Riga, 1974
6. USSR P. 1 611 861; *Byull. Izobret.* (45) 123 (1990)
7. M R Suvorova, E L Gabova, T V Sorokina, L N Kalitina, N I Berg, I A Leont'eva *Tekhnol. Bornykh Soedin.* **40** 70 (1976)
8. USSR P. 1 024 866; *Byull. Izobret.* (23) 151 (1983)
9. H Rawson *Inorganic Glass-Forming Systems* (London; New York: Academic Press, 1967)
10. E M Levin, H F McMurdie, C R Robbins *Phase Diagrams for Ceramics* (Washington, DC: NBS, 1964)
11. N A Toropov, V P Bazarkovskii, V V Lapin, N N Kurtseva *Diagrammy Sostoyaniya Silikatnykh Sistem. Spravochnik* (State Diagrams of Silicate Systems. Handbook) (Leningrad: Nauka, 1969)
12. E M Levin, H F McMurdie *J. Res. Nat. Bur. Stand.* **42** 131 (1949)
13. E M Levin, G M Urginic *J. Res. Nat. Bur. Stand.* **51** 37 (1953)
14. O V Mazurin, M V Strel'tsina, T P Shvaiko-Shvaikoskaya *Svoistva Stekol i Stekloobrazuyushchikh Rasplavov. Spravochnik* (Properties of Glasses and Glass Forming Solutions. Handbook) (Leningrad: Nauka, 1975) Vol. 2
15. N I Leonyuk, L I Leonyuk *Kristallokhimiya Bezvodnykh Boratov* (Crystal Chemistry of Anhydrous Borates) (Moscow: Moscow State University, 1983)
16. S Block, A Perloff *Acta Crystallogr.* **19** 297 (1965)
17. A D Mighell, A Perloff *Acta Crystallogr.* **20** 819 (1966)
18. J Krogh-Moe, M Ihara *Acta Crystallogr., Sect. B* **25** 2153 (1969)
19. H B Gray *Electrons and Chemical Bonding* (New York; Amsterdam: W A Benjamin, 1965)
20. C Chen, B Wu, A Jiang, G You *Sci. Sinica, B* **28** 235 (1985)
21. C Chen, G Liu *Annu. Rev. Mater. Sci.* **16** 203 (1986)
22. S Lu, M Ho, J Huang *Wuli Xuebao (Acta Phys. Sinica)* **31** 948 (1982)
23. J-R Liang, Y-L Zhang, A-Z Huang *Acta Chem. Sinica.* **40** 994 (1982)
24. D Y Tang, S T Ling *J. Synt. Crystals* **14** 148 (1985)
25. A D Jiang, F Cheng *J. Synt. Crystals* **14** 149 (1985)
26. L A Shuvalov, A A Urusovskaya, I S Zheludev, A V Zalesskii, S A Semiletov, B N Grechushnikov, I G Chistyakov, S A Pikin *Sovremennaya Kristallografiya. Fizicheskie Svoistva Kristallov* (Modern Crystallography. Physical Properties of Crystals) (Moscow: Nauka, 1981) Vol. 4
27. A A Blistanov *Kristally Kvantovoi i Nelineinoi Optiki* (Crystals of Quantum and Nonlinear Optics) (Moscow: Moscow Institute of Steel and Alloys, 2000)
28. V V Osiko, T T Basiev, in *IX Natsional'naya Konferentsiya po Rostu Kristallov (Tez. Dokl.)* [(The IXth National Conference on Growth of Crystals (Abstracts of Reports)] (Moscow: Institute of Catalysis, Russian Academy of Sciences, 2000) p. 7
29. T T Basiev *Usp. Fiz. Nauk* **169** 1149 (1999) [*Phys.-Usp.* **42** 1051 (1999)]
30. A A Kaminskii, S N Bagaev, A M Yurkin, A E Kokh, G Eikhler, Yu Findaizen *Dokl. Akad. Nauk* **367** 468 (1999) [a]
31. C Chen, Y Wu, A Jiang, B Wu, G You, R Li, S Lin *J. Opt. Soc. Am. B* **6** 616 (1989)
32. C Chen, Z Xu, D Deng, J Zhang, G K L Wong, Y Wu, N Ye, D Tang *Appl. Phys. Lett.* **68** 2930 (1996)
33. C Chen, Y Wang, B Wu, K Wu, W Zeng , L Yu *Nature (London)* **373** 322 (1995)
34. Y Mori, I Kuroda, S Nakajima, T Sasaki, S Nakai *Appl. Phys. Lett.* **67** 1818 (1995)
35. N Ye, Z Weng, B Wu, C Chen *Proc. SPIE-Int. Soc. Opt. Eng.* **3556** 156 (1998).
36. P Becker, J Liebertz, L Bohaty *J. Cryst. Growth* **203** 149 (1999)
37. C Chen, Y Wu, R Li *J. Cryst. Growth* **99** 790 (1990)
38. C Chen *J. Synt. Cryst. (China)* **30** 36 (2001)
39. L I Isaenko, A P Eliseev *Khim. Inter. Ustoich. Razvit.* **8** 103 (2000) [b]
40. R H French, J W Ling, F S Ohuchi, C T Chen *Phys. Rev. B* **44** 8496 (1991)
41. W-D Cheng, J-X Lu *Chinese J. Struct. Chem.* **16** 81 (1997)
42. J Lin, M-H Lee, Z-P Liu, C Chen, Ch J Pickard *Phys. Rev. B* **60** 13 380 (1999)
43. D Xue, K Betzler, H Hesse, D Lammers *Solid State Commun.* **114** 21 (2000)
44. D Elmeri, L Davis, S Velsko, E K Graham, A Zalkin *J. Appl. Phys.* **62** 1966 (1987)
45. L K Cheng, W Bosenberg, C L Tang *Prog. Cryst. Growth Charact.* **20** 9 (1990)
46. R S Feigelson, R J Raymakers, R K Route *Prog. Cryst. Growth Charact.* **20** 115 (1990)
47. W Eitel *The Physical Chemistry of the Silicates* (Chicago: University of Chicago Press, 1954)
48. N I Leonyuk *J. Cryst. Growth* **174** 301 (1997)
49. V P Soltsev, E G Tsvetkov, V A Gets, V D Antsygin *J. Cryst. Growth* **236** 290 (2002)
50. U Sborgi *Atti Reale Acad. Naz. Linc., Sec. 5* **28** 854 (1914)
51. H-A Lehmann, K Muhmel, Dzui-Fang Sun *Z. Anorg. Allg. Chem.* **355** 238 (1967)
52. V B Kravchenko *Zh. Strukt. Khim.* **6** 724 (1965) [c]
53. L Kutschabsky *Acta Crystallogr., Serct. B* **25** 1811 (1969)
54. V I Simonov, O G Karpov, Ya Ya Shvirkst, G K Gode *Kristallografiya* **34** 1292 (1989) [d]
55. D Yu Pushcharovsky, S Merlino, O Ferro, S A Vinigradova, O V Dimitrova *J. Alloys Compd.* **306** 163 (2000)
56. O Ferro, S Merlino, S A Vinigradova, D Yu Pushcharovsky, O V Dimitrova *J. Alloys Compd.* **305** 63 (2000)
57. A V Arakcheeva, S A Vinogradova, D Yu Pushcharovskii, M Khostettler, Zh Shapui, O V Dimitrova *Kristallografiya* **45** 448 (2000) [d]
58. O V Dimitrova, in *Kristallogenezis i Mineralogiya (Tez. Dokl.)* [Crystallogenesis and Mineralogy (Abstracts of Reports)] (S Petersburg: S Petersburg University, 2001) p. 92
59. W Guertler *Z. Anorg. Chem.* **40** 343 (1904)
60. F de Carli *Atti Reale Acad. Naz. Linc., Sec. 6* **5** 44 (1927)
61. V B M Hageman, H A J Oonk *Phys. Chem. Glasses* **20** 126 (1979)
62. K-H Hübner *Neues Jahrbuch Mineralog. Monatsh.* 335 (1969)

63. Jpn. P. 249 698 (A); *Izobreteniya Stran Mira* (Inventions of World States) (Moscow: All-Russian Research Institute of Patent Information, 1990)
64. V Nikolov, P Peshev *J. Solid. State Chem.* **96** 48 (1992)
65. K-H Hübner *Neues Jahrbuch Mineralog. Abhandl.* **112** 150 (1970)
66. A B Bykov, V V Dozmarov, O K Mel'nikov *Kristallografiya* **39** 720 (1994)
67. C B Robbins, E M Levin *J. Res. Natl. Bur. Stand. A* **73** 615 (1969)
68. J L Stone, A Keszler, G Aka, A Kahn-Harari, T A Reynolds *Proc. SPIE-Int. Soc. Opt. Eng.* **4268** 175 (2001)
69. J Liebertz, S Stahr *Z. Kristallogr.* **165** 91 (1983)
70. R Frohlich *Z. Kristallogr.* **168** 109 (1984)
71. K Ito, F Marumo, M Ohgaki, K Tanaka *Res. Lab. Eng. Mater. Tokyo Inst. Technol.* **15** 1 (1990)
72. R Sole, V Nikolov, M C Pujol, J Gavalda, X Ruiz, J Massons, M Aguilo, F Diaz *J. Cryst. Growth* **207** 104 (1999)
73. *Powder Diffraction File Card 15-0862, JCPDS* (Swartmore, PA: International Center of Diffraction Data)
74. *Powder Diffraction File Card 44-0584, JCPDS* (Swartmore, PA: International Center of Diffraction Data)
75. C E Weir, R A Schroeder *J. Res. Nat. Bur. Stand. A* **68** 465 (1964)
76. I Wozniak, P F James *Glass Technol.* **25** 98 (1984)
77. E M Shvarts, A E Dzene, in *Boraty i Boratnye Sistemy* (Borates and Borate Systems) (Ed. G Ya Slaidin) (Riga: Zinatne, 1978) p. 101
78. A F Nikolaev *Fiziko-Khimicheskoe Izuchenie Prirodnykh Boratov* (Physicochemical Study of Natural Borates) (Moscow: Izd. Akad. Nauk SSSR, 1947)
79. K Itoh, F Marumo, Y Kuwana *J. Cryst. Growth* **106** 728 (1990)
80. H Kouta, Y Kuwana, K Ito, F Marumo *J. Cryst. Growth* **114** 676 (1991)
81. S Imoto, S Kimura, Y Anzai, Y Kuwano *J. Cryst. Growth* **135** 279 (1994)
82. N Yoshimoto, S Kimura *J. Cryst. Growth* **144** 229 (1994)
83. D M Schleich *Solid State Ion.* **79**/**71** 407 (1994)
84. O Yamaguchi, K Tominaga, K Shimizu *Ceramurg. Int.* **6** 103 (1980)
85. L I Ivleva, D T Kiselev, Yu S Kuz'minov, V V Voronov, N M Polozkov *Izv. Akad. Nauk SSSR, Neorg. Mater.* **24** 1153 (1988)
86. L K Cheng, W Bosenberg, C L Tang *J. Cryst. Growth* **89** 553 (1988)
87. K L Ovanesyan, A G Petrosyan, G O Shirinyan *Cryst. Res. Technol.* **24** 859 (1989)
88. T Katsumata, H Ishijima, T Sugano, M Yamagishi, K Takahashi *J. Cryst. Growth* **123** 597 (1992)
89. H Kimura, T Numazawa, M Sato *J. Cryst. Growth* **165** 408 (1996)
90. E G Tsvetkov, A M Yurkin *Kristallografiya* **43** 1142 (1998) [d]
91. E G Tsvetkov, A A Tomilenko, G G Khranenko, A M Yurkin *Kristallografiya* **45** 762 (2000) [d]
92. L I Ivleva, I G Gordadze, Yu S Kuz'minov, V V Voronov, V M Ivanovskaya *Izv. Akad. Nauk SSSR, Neorg. Mater.* **25** 804 (1989) [e]
93. L H Brixner, K Babcock *Mater. Res. Bull.* **3** 817 (1968)
94. Jpn. P. 63-18 755 (A); *Izobr. Stran Mira* **72** (MKI 130) (6) 13 (1990)
95. *Powder Diffraction File Card 1-0861, JCPDS* (Swartmore, PA: International Center of Diffraction Data)
96. M Marezio, H A Plettinger, W H Zachariasen *Acta Crystallogr.* **16** 594 (1963)
97. J Q Lu, G X Lan, B Li, Y Y Yang, H F Wang, B C Wu *J. Phys. Chem. Solids* **49** 519 (1988)
98. J Liebertz *Z. Kristallogr.* **182** 307 (1988)
99. Yu K Voronko, A V Gorbachev, V V Osiko, A A Sobol, R S Feigelson, R K Route *J. Phys. Chem. Solids* **54** 1579 (1993)
100. Yu K Voron'ko, A V Gorbachev, A A Sobol', L I Tsymbal *Neorg. Mater.* **30** 646 (1994) [e]
101. A E Kokh, N G Kononova, P P Fedorov, V S Boyarkov, R M Zakalyukin, V A Chubarenko *Kristallografiya* **48** 616 (2002) [d]
102. P P Fedorov, N G Kononova, A E Kokh, A A Sobol', Yu F Kargin, V S Boyarkov, R M Zakalyukin, E A Tkachenko *Zh. Neorg. Khim.* **47** 1150 (2002) [f]
103. A Jiang, F Cheng, Q Lin, G Cheng, Y Zheng *J. Cryst. Growth* **79** 963 (1986)
104. A F Selevich, E E Vershel', in *Aktual'nye Voprosy Sovremennoi Khimii (Tez. Dokl. 2-oi Respubl. Konf. Molodykh Uchenykh i Spetsialistov)* [Topical Problems of Modern Chemistry (Abstracts of Reports of the Second Republican Conference of Young Scientists and Specialists)] (Minsk: Belorussia State University, 1991) p. 33
105. Q-Z Huang, J K Liang *Acta Phys. Sin.* **30** 559 (1981)
106. Y Kozuki, M Itoh *J. Cryst. Growth* **114** 683 (1991)
107. H Kimura, R S Feigelson *J. Alloys Compd.* **234** 187 (1996)
108. J Liebertz, R Frohlich *Z. Kristallogr.* **168** 293 (1984)
109. X Huang, Y Zhao, K Lu, D Tang *J. Cryst. Growth* **165** 413 (1996)
110. P P Fedorov, B P Sobolev *Zh. Fiz. Khim.* **62** 896 (1988) [g]
111. G H Rao, J K Liang, Z Y Qiao, Q Z Huang *CALPHAD, Comput. Coupling Phase Diagr. Thermochem.* **13** 169 (1989)
112. Yu K Voron'ko, A V Gorbachev, A B Kudryavtsev, V V Osiko, A A Sobol' *Neorg. Mater.* **28** 1713 (1992) [e]
113. S Takeda, S Kimura, K Sugiyama *High Temp. Mater. Process* **10** 209 (1992)
114. H Ogawa, Y Waseda *J. Cryst. Growth* **128** 945 (1993)
115. Sangeeta, S C Sabharwal *J. Cryst. Growth* **222** 427 (2001)
116. H Kimura, T Numazawa, M Sato *J. Cryst. Growth* **174** 308 (1997)
117. K-T Vil'ke *Vyrashchivanie Kristallov* (Crystal Growing) (Leningrad: Nedra, 1977)
118. A A Chernov, E I Givargizov, Kh S Bagdasarov, L N Dem'yanets, V A Kuznetsov, A N Lobachev *Sovremennaya Kristallografiya. Obrazovanie Kristallov* (Modern Crystallography. Crystal Formation) (Moscow: Nauka, 1980) Vol. 3
119. V A Timofeeva *Rost Kristallov iz Rastvorov-Rasplavov* (Crystal Growth from Solution-Melts) (Moscow: Nauka, 1978)
120. D Y Tang, R K Route, R S Feigelson *J. Cryst. Growth* **91** 81 (1988)
121. D Y Tang, W R Zeng, Q L Zhao *J. Cryst. Growth* **123** 445 (1992)
122. A B Kaplun, E N Galashov, G D Vshivkova *Neorg. Mater.* **27** 1723 (1994) [e]
123. M Roth, N Angert, M Tseitlin, G Wang, T P J Han, H G Gallaher, N I Leonyuk, E V Koporulina, S N Barilo, L A Kurnevich, in *The 3rd International Conference on Single Crystal Growth, Strength Problems, and Heat Mass Transfer (Abstracts of Reports), Obninsk, 1999* p. 67
124. Q Huang, J Luang *J. Cryst. Growth* **97** 720 (1989)
125. D M Gualtieri, B H-T Chai, M H Randles *J. Cryst. Growth* **97** 613 (1989)
126. A B Kaplun, A B Meshalkin *Neorg. Mater.* **31** 1602 (1995) [e]
127. P F Bordui, G D Calvert, R Blachman *J. Cryst. Growth* **129** 371(1993)
128. E G Rakov, V V Teslenko *Pirogidroliz Neorganicheskikh Ftoridov* (Pyrohydrolysis of Inorganic Fluorides) (Moscow: Energoatomizdat, 1987)
129. S N Barilo, A P Ges, S A Guretskii *J. Cryst. Growth* **108** 309 (1991)
130. R S Feigelson, R J Raymakers, R K Route *J. Cryst. Growth* **97** 352 (1989)
131. R Oude Hengel, F Fischer *J. Cryst. Growth* **114** 656 (1991)
132. D Perlov, M Roth *J. Cryst. Growth* **137** 123 (1994)
133. A B Kaplun, E N Galashov, G D Vshivkova, A B Meshalkin *Neorg. Mater.* **30** 521 (1994) [e]
134. A M Luginets, S A Guretskii, A P Ges, A S Milovanov, L V Markova, V S Burak *J. Cryst. Growth* **162** 89 (1996)
135. V Nikolov, P Peshev, Kh Khubanov *J. Solid State Chem.* **97** 36 (1992)
136. V Nikolov, P Peshev *J. Cryst. Growth* **147** 117 (1995)
137. RF P. 2 139 957; *Byull. Izobret.* (29) (1999)
138. A E Kokh, V A Mishchenko, V D Antsigin, A M Yurkin, N G Kononova, V A Guets, Y K Nizienko, A I Zakharchenko *Proc. SPIE-Int. Soc. Opt. Eng.* **3610** 139 (1999)
139. A E Kokh, N G Kononova *J. Cryst. Growth* **198**/**199** 161 (1999)
140. A E Kokh, N G Kononova, P W Mokruchnikov *J. Cryst. Growth* **216** 359 (2000)
141. A E Kokh, V A Gets, A M Yurkin, O S Il'ina, E G Samoilova, in *Tezisy Dokladov Vtoroi Konferentsii 'Materialy Sibiri'* (Abstracts of Reports of the Second Conference 'Materials of Siberia') (Barnaul: Altai State Technology Institute, 1998) p. 145

142. N G Kononova, A E Kokh, in *IX Natsional'naya Konferentsiya po Rostu Kristallov (Tez. Dokl.)* [The IXth National Conference on Crystal Growth (Abstracts of Reports)] (Moscow: Institute of Catalysis, Russian Academy of Sciences, 2000) p. 456
143. V I Tyurikov, E G Tsvetkov, G G Khranenko *Poverkhnost'* (5) 40 (2002)
144. E G Tsvetkov, V I Tyurikov *Proc. SPIE-Int. Soc. Opt. Eng.* **4268** 186 (2001)
145. X Hong, K Lu, L Li, D Tang *J. Cryst. Growth* **193** 610 (1998)
146. W R Bosenberg, R J Lane, C L Tang *J. Cryst. Growth* **108** 394 (1991)
147. A Kokh *J. Cryst. Growth* **191** 774 (1998)
148. RF P. 2 133 786; *Byull. Izobret.* (21) (1999)
149. A E Kokh, V E Kokh, V N Gets, N G Kononova *Pribory Tekhn. Eksp.* **1** 153 (1998)
150. A E Kokh, V E Kokh, N G Kononova *Pribory Tekhn. Eksp.* **1** 157 (2000)
151. A E Kokh, N G Kononova *Solid-State Electron.* **44** 819 (2000)
152. RF P. 2 163 943; *Byull. Izobret.* (7) (2001)
153. RF P. 2 164 561; *Byull. Izobret.* (9) (2001)
154. A E Kokh, N G Kononova, V N Popov, P W Mokruchnikov *Proc. SPIE-Int. Soc. Opt. Eng.* **4268** 161 (2001)
155. P A Morris *J. Cryst. Growth* **106** 76 (1990)
156. N S Stel'makh, V E Kritskaya, G N Pirogova *Neorg. Mater.* **32** 995 (1996) [e]
157. J Hou, Q Tan, Q Zhao, B Wu, C Chen *Appl. Phys. Lett.* **58** 1149 (1991)
158. A Peter, K Polgar, E Beregi *J. Cryst. Growth* **209** 102 (2000)
159. S C Sabharwal, Sangeeta, M Goswami, S K Kulkarni, B D Padalia *J. Mater. Sci., Mater. Electron.* **11** 325 (2000)
160. S C Sabharwal, Sangeeta *J. Cryst. Growth* **187** 253 (1998)
161. Q Tan, H Mao, S Lin, C Chen, S Lu, D Tang, T Ogawa *J. Cryst. Growth* **141** 393 (1994)
162. B Chalmers *Principles of Solidification* (New York: Wiley, 1964)
163. M C Flemings *Solidification Processing* (New York: McGraw-Hill, 1974)
164. S R Corriel, G B McFadden, R F Sekerka *Annu. Rev. Mater. Sci.* **15** 119 (1985)
165. J D Weeks, W Vansaarloos, M Grant *J. Cryst. Growth* **112** 244 (1991)
166. P P Fedorov *Neorg. Mater.* **37** 95 (2001) [e]
167. J S Kirkaldy, L C Brown *Can. Metall. Q.* **2** 89 (1963)
168. Z Cheng, Y Lei, D Tang *J. Cryst. Growth* **183** 227 (1998)
169. G C Bhar, S Das, U Chatterjee *Appl. Opt.* **28** 2 (1989)
170. M Brown *Opt. Lett.* **23** 1591 (1998)
171. C L Tang, W R Bosenberg , T Ukachi, R J Lane, L K Cheng *Laser Focus World* **10** 107 (1990)
172. K Kato *IEEE J. Quantum Electron.* **22** 1013 (1986)
173. S Imai, T Yamada, Y Fujimori, K Ishikawa *Appl. Phys. Lett.* **54** 1206 (1989)
174. A Dubietis, G Tamosauskas, A Varanavicius, G Valiulis *Appl. Opt.* **39** 2437 (2000)
175. P S Banks, M D Feit, M D Perry *Opt. Lett.* **24** 4 (1999)
176. C Droz, H Kouta, Y Kuwano *Opt. Rev.* **6** 97 (1999)
177. H Kouta, Y Kuwano *Opt. Lett.* **24** 1230 (1999)
178. G C Bhar, U Chatterjee, A M Rudra, P Kumbkhakar *Kvant. Elektr.* **29** 800 (1999) [*Quant. Electr.* **29** 800 (1999)]
179. J D Bhavalkar, Y Mao, H Po, A K Goyal, P Gavrilovic, Y Conturie, S Singh *Opt. Lett.* **24** 823 (1999)
180. K Matsubara, U Tanaka, H Imajo, M Watanabe, S Urabe *J. Opt. Soc. Am. B* **16** 1668 (1999)
181. T Zhang, K Yamakawa *Jpn. J. Appl. Phys.* **39** 91 (2000)
182. W Joosen, H J Bakker, L D Noordam, H G Muller, H B van Linden van den Heuvell *J. Opt. Soc. Am. B* **8** 2087 (1991)
183. R Wu *Appl. Opt.* **32** 971 (1993)
184. Z Y Min, R W Quandt, R Bersohn, H L Kim *IEEE J. Quantum Electron.* **34** 2409 (1998)
185. W R Bosenberg, W S Pelouch, C L Tang *Appl. Phys. Lett.* **55** 1952 (1989)
186. A Borsutzky, R Brunger, Ch Huang, R Wallenstein *Appl. Phys. B* **52** 55 (1991)
187. Y Taira *Jpn. J. Appl. Phys.* **31** L682 (1992)
188. G C Bhar, S Das, U Chatterjee *J. Phys. D* **22** 562 (1989)
189. G C Bhar, S Das, U Chatterjee *Appl. Phys. Lett.* **54** 1383 (1989)
190. G C Bhar, P Kumbhakar, U Chatterjee, A M Rudra, Y Kuwano, H Kouta *Appl. Opt.* **37** 7827 (1998)
191. G C Bhar, P Kumbhakar, U Chatterjee, A M Rudra, Y Kuwano, H Kouta *Appl. Opt.* **38** 1802 (1999).
192. A Fix, T Schroder, R Wallenstein *Laser Optoelectron.* **23** 106 (1991)
193. W R Bosenberg, L K Cheng, C L Tang *Appl. Phys. Lett.* **54** 13 (1989)
194. N V Kondratyuk, A A Shagov, K L Demidchik, A M Yurkin, Aleksandr E Kokh *Kvant. Elektr.* **30** 253 (2000) [*Quant. Electr.* **30** 253 (2000)]
195. V D Antsygin, V A Gusev, A M Yurkin *Avtometriya* **3** 16 (1996)
196. V D Antsygin *Avtometriya* **1** 24 (1998)
197. V T Adamiv, Ya V Burak, Ya O Dovgii, I V Kityk *Kristallografiya* **36** 229 (1991) [d]
198. S-L Hong, B-C Wu *Opt. Eng.* **34** 1738 (1995)
199. J D Beasley *Appl. Opt.* **33** 1000 (1994)
200. H Kouta *Appl. Opt.* **38** 545 (1999)
201. H Kouta, Y Kuwano *Appl. Opt.* **38** 1053 (1999)

[a] — *Dokl. Chem. (Engl. Transl.)*
[b] — *Chem. Sustain. Dev. (Engl. Transl.)*
[c] — *Russ. J. Struct. Chem. (Engl. Transl.)*
[d] — *Crystallogr. Rep. (Engl. Transl.)*
[e] — *Inorg. Mater. (Engl. Transl.)*
[f] — *Russ. J. Inorg. Chem. (Engl. Transl.)*
[g] — *Russ. J. Phys. Chem. (Engl. Transl.)*